Spin and charge dynamics of the ferromagnetic and antiferromagnetic two-dimensional half-filled Kondo lattice model

S. Capponi and F. F. Assaad
Institut für Theoretische Physik III, Universität Stuttgart, Pfaffenwaldring 57, D-70550 Stuttgart, Germany
(Received 26 October 2000; published 30 March 2001)

We present a detailed numerical study of ground state and finite temperature spin and charge dynamics of the two-dimensional Kondo lattice model with hopping t and exchange J. Our numerical results stem from auxiliary field quantum Monte Carlo simulations formulated in such a way that the sign problem is absent at half-band filling thus allowing us to reach lattice sizes up to 12×12. At $T=0$ and antiferromagnetic couplings $J>0$ the competition between the Ruderman-Kittel-Kasuya-Yosida interaction and the Kondo effect triggers a quantum phase transition between antiferromagnetically ordered and magnetically disordered insulators: $J_c/t=1.45\pm 0.05$. At $J<0$ the system remains an antiferromagnetically ordered insulator and irrespective of the sign of J, the quasiparticle gap scales as $|J|$. The dynamical spin structure factor $S(\vec{q},\omega)$ evolves smoothly from its strong-coupling form with spin gap at $\vec{q}=(\pi,\pi)$ to a spin-wave form. For $J>0$, the single-particle spectral function $A(\vec{k},\omega)$ shows a dispersion relation following that of hybridized bands as obtained in the noninteracting periodic Anderson model. In the ordered phase this feature is supplemented by shadows, thus allowing an interpretation in terms of the coexistence of Kondo screening and magnetic ordering. In contrast, at $J<0$ the single-particle dispersion relation follows that of noninteracting electrons in a staggered external magnetic field. At finite temperatures spin T_S and charge T_C scales are defined by locating the maximum in the charge and spin uniform susceptibilities. For weak to intermediate couplings, T_S marks the onset of antiferromagnetic fluctuations—as observed by a growth of the staggered spin susceptibility—and follows a J^2 law. At strong couplings T_S scales as J. On the other hand T_C scales as J both in the weak- and strong-coupling regime. At and slightly below T_C we observe (i) the onset of screening of the magnetic impurities, (ii) a rise in the resistivity as a function of decreasing temperature, (iii) a dip in the integrated density of states at the Fermi energy, and finally (iv) the occurrence of hybridized bands in $A(\vec{k},\omega)$. It is shown that in the weak-coupling limit, the charge gap of order J is formed only at T_S and is hence of magnetic origin. The specific heat shows a two-peak structure. The low-temperature peak follows T_S and is hence of magnetic origin. Our results are compared to various mean-field theories.

DOI: 10.1103/PhysRevB.63.155114 PACS number(s): 71.27.+a, 71.10.Fd

I. INTRODUCTION

The Kondo lattice model (KLM) as well as the periodic Anderson model (PAM) are the prototype Hamiltonians to describe heavy fermion materials[1] and Kondo insulators.[2] The physics under investigation is that of a lattice of magnetic impurities embedded in a metallic host. The symmetric PAM reads

$$H_{PAM}=\sum_{\vec{k},\sigma}\varepsilon(\vec{k})c^{\dagger}_{\vec{k},\sigma}c_{\vec{k},\sigma}-V\sum_{\vec{i},\sigma}(c^{\dagger}_{\vec{i},\sigma}f_{\vec{i},\sigma}+f^{\dagger}_{\vec{i},\sigma}c_{\vec{i},\sigma})+U_f\sum_{\vec{i}}(n^{f}_{\vec{i},\uparrow}-1/2)(n^{f}_{\vec{i},\downarrow}-1/2). \quad (1)$$

The unit cell, denoted by $\vec{i}$, contains an extended and a localized orbital. The fermionic operators $c^{\dagger}_{\vec{k},\sigma}$ ($f^{\dagger}_{\vec{k},\sigma}$) create electrons on extended (localized) orbitals with wave-vector $\vec{k}$ and z component of spin σ. The overlap between extended orbitals generates a conduction band with dispersion relation $\varepsilon(\vec{k})$. There is a hybridization matrix element V between both orbitals in the unit cell and the Coulomb repulsion—modeled by a Hubbard U_f—is taken into account on the localized orbitals. In the limit of large U_f, charge fluctuations on the localized orbitals are suppressed and the PAM maps onto the KLM:[3]

$$H_{KLM}=\sum_{\vec{k},\sigma}\varepsilon(\vec{k})c^{\dagger}_{\vec{k},\sigma}c_{\vec{k},\sigma}+J\sum_{\vec{i}}\vec{S}^{c}_{\vec{i}}\cdot\vec{S}^{f}_{\vec{i}}. \quad (2)$$

Here, $\vec{S}^{c}_{\vec{i}}=\frac{1}{2}\Sigma_{s,s'}c^{\dagger}_{\vec{i},s}\vec{\sigma}_{s,s'}c_{\vec{i},s'}$, where $\vec{\sigma}$ are the Pauli $s=1/2$ matrices. A similar definition holds for $\vec{S}^{f}_{\vec{i}}$. A magnetic energy scale $J=8V^2/U$ emerges and there is a constraint of one electron per localized orbital. Although this constraint forbids charge fluctuations on the localized orbitals, those fluctuations are implicitly taken into account leading to the above form and sign of the exchange interaction. On the other hand, when charge fluctuations on the localized orbitals are absent, the exchange interaction follows from Hund's rule and is ferromagnetic. The ferromagnetic KLM has attracted much attention in conjunction with manganites.[4] In this paper we will consider both ferromagnetic and antiferromagnetic exchange interactions with emphasis on the antiferromagnetic case.

The physics of the single impurity Anderson and Kondo models at $J/t>0$ is well understood.[5] In the temperature range $J<T<U$, charge is localized on the f orbital, but the spin degrees of freedom are essentially free, thus leading to a

Curie-Weiss law for the impurity spin susceptibility. Below the Kondo temperature $T_K \propto \varepsilon_f e^{-1/JN(\varepsilon_f)}$ the impurity spin is screened by the conduction electrons. Here, ε_f is the Fermi energy and $N(\varepsilon_f)$ the density of states taken at the Fermi energy. The transition from high to low temperatures is nonperturbative and corresponds to the Kondo problem with the known resistivity minimum[6] and orthogonality catastrophe.[7] At low temperatures, T_K is the only energy scale in the problem.

A lattice of magnetic impurities introduces new energy scales. In the spin sector, the Ruderman-Kittel-Kasuya-Yosida (RKKY) interaction[8] couples impurity spins via polarization of the conduction electrons. This interaction takes the form of a Heisenberg model with exchange $J_{eff}(\vec{q}) \propto -J^2 \,\mathrm{Re}\,\chi(\vec{q},\omega=0)$ where $\chi(\vec{q},\omega)$ corresponds to the spin susceptibility of the conduction electrons. Since this interaction favors magnetic ordering, it freezes the impurity spins and, hence, competes with the Kondo effect. By comparing energy scales, one expects the RKKY interaction (Kondo effect) to dominate at weak (strong) couplings. As suggested by Doniach,[9] this leads to a quantum phase transition between ordered and disordered magnetic phases.

As a function of dimension, contrasting results are obtained for the PAM and KLM. We first consider the limit of large dimensions[10,11] and the Gutzwiller approximation.[12] The Gutzwiller approximation leads to an noninteracting PAM with renormalized hybridization V. At half filling an insulating state is obtained, with quasiparticle gap $\sim e^{-1/2JN(\varepsilon_f)}$ in the large U_f limit. Both the Gutzwiller and dynamical mean-field approaches yield charge and spin gaps equal to each other. As a function of temperature, optical and quasiparticle gaps start appearing at an energy scale $\sim e^{-1/2JN(\varepsilon_f)}$.[10] In the doped phase, the Luttinger volume includes the f electrons, and due to the renormalization of the hybridization, the effective mass of charge carriers is enhanced. The above quoted results stem from calculations for the PAM. However, similar results are obtained in the framework of the KLM at $J/t \ll 1$ in the limit of large dimensions.[11] The above approximations predict an instability to magnetic ordering in the large U_f or small J limit. The occurrence of this instability has been observed in the framework of quantum Monte Carlo (QMC) simulations of the PAM in two dimensions.[13,14] In the one-dimensional case, a good understanding of the phase diagram of the KLM as a function of electronic density and coupling has been achieved.[15,16] In particular, at half filling, a spin liquid phase is obtained irrespective of the value of J/t. In the weak-coupling limit the spin gap follows a Kondo form, whereas the charge gap tracks J.

In this paper, we present a detailed numerical study of ground-state and finite-temperature properties of the half filled KLM in intermediate dimensions, $d=2$. Our $T=0$ simulations are aimed at understanding the competition and interplay of the Kondo effect and RKKY interaction. Our finite temperature simulations provide insight into the temperature evolution of spin and charge degrees of freedom.

Our main results and structure of the article is as follows. Details of the numerical technique are presented in the next section. We use a path integral auxiliary field quantum Monte Carlo (QMC) method.[17] Our approach is based on a simple technical innovation that allows us to avoid the sign problem at least at half band filling where the model is particle-hole symmetric. Both finite- and zero-temperature versions of the algorithm are presented. In both cases imaginary time displaced correlations functions can be computed. The continuation to real time is then carried out via the use of the maximum entropy (ME) method.[18] We note that the algorithms may be applied irrespective of the sign of J.

In Sec. III, ground-state equal time and dynamical properties of the ferromagnetic and antiferromagnetic KLM are presented. Our main results include the following. (i) In the spin sector, a quantum phase transition between antiferromagnetically ordered and disordered ground states occurs at $J/t=1.45\pm0.05$. The dynamical spin structure factor is analyzed across the transition. As a function of decreasing values of J/t, the spin gap at the antiferromagnetic wave vector closes and the magnon spectrum evolves towards a spin-wave form. This spin-wave form persists for ferromagnetic couplings since in the limit $J/t\to\infty$, the model maps onto the $s=1$ antiferromagnetic Heisenberg model. Our results at $J/t>0$ are compared to a bond-operator mean-field theory of the Kondo necklace model. (ii) In the charge sector, the system remains an insulator. To a first approximation, the quasiparticle gap tracks J both in the antiferromagnetic and ferromagnetic KLM. For all values of $J/t>0$ the single-particle spectral function shows a feature whose dispersion relation follows the one obtained in the noninteracting PAM. In a mean-field approach, this feature results solely from Kondo screening of the magnetic impurities. In the magnetically ordered phase, this feature is supplemented by shadow bands. Thus, and as confirmed by a mean-field approach, the spectral function in the ordered phase may only be understood in terms of the coexistence of Kondo screening and the RKKY interaction. On the other hand, at $J/t<0$, where Kondo screening is absent, the single-particle dispersion relation follows that of free electrons in a external staggered magnetic field.

Section IV is devoted to finite temperature properties of the KLM. We define charge T_C, as well as spin T_S scales from the location of the maximum in the charge and spin susceptibilities. In the weak- and strong-coupling limit, the charge scale tracks J. On the other hand the spin scale—as expected form the energy scale associated to the RKKY interaction—follows a J^2 law up to intermediate couplings. At strong couplings $T_S \propto J$. Since T_C corresponds to the energy scale at which a minimum in the resistivity is observed, we conclude that it describes the energy scale at which scattering is enhanced due to the screening of the impurity spins. Furthermore a reduction of the integrated density of states at the Fermi level is observed at T_C. The spin scale up to intermediate couplings (i.e., $J/t \leqslant W$ where W corresponds to the bandwidth) marks the onset of short-range antiferromagnetic correlations. This is confirmed by the calculation of the staggered spin susceptibility that shows a strong increase at T_S. In the weak-coupling limit, it is shown that the quasiparticle gap of magnitude $\propto J$ is formed only at the magnetic energy scale T_S and, is thus, of magnetic origin. In the tem-

perature range $T_S<T<T_C$ hybridized band are seen in the single-particle spectral function with quasiparticle gap lying beyond our resolution. Finally, the specific heat is computed and shows a two-peak structure. The low-energy peak tracks the spin scale and, is hence, of magnetic origin. In the last section, we discuss our results, as well as links with experiments.

II. AUXILIARY FIELD QUANTUM MONTE CARLO ALGORITHM FOR THE KONDO LATTICE MODEL

Auxiliary field QMC simulations of the KLM, as well as the two-impurity Kondo model have already been carried out by Fye and Scalapino.[19,20] However, their formulation leads to a sign problem even in the half-filled case where the model is invariant under a particle-hole transformation. In this section we present an alternative formulation of the problem that is free of the sign problem in the particle-hole symmetric case. In order to achieve our goal, we take a detour and consider the Hamiltonian:

$$H=\sum_{\vec{k},\sigma}\ \varepsilon(\vec{k})c^{\dagger}_{\vec{k},\sigma}c_{\vec{k},\sigma}-\frac{J}{4}\sum_{\vec{i}}\ \left[\sum_{\sigma}\ c^{\dagger}_{\vec{i},\sigma}f_{\vec{i},\sigma}+f^{\dagger}_{\vec{i},\sigma}c_{\vec{i},\sigma}\right]^2. \tag{3}$$

As we will see below, at vanishing chemical potential, this Hamiltonian has all the properties required to formulate a sign-free auxiliary field QMC algorithm. Here, we are interested in the ground-state properties of H that we obtain by filtering out the ground state $|\Psi_0\rangle$ by propagating a trial wave function $|\Psi_T\rangle$ along the imaginary time axis:

$$\frac{\langle\Psi_0|O|\Psi_0\rangle}{\langle\Psi_0|\Psi_0\rangle}=\lim_{\Theta\to\infty}\frac{\langle\Psi_T|e^{-\Theta H}Oe^{-\Theta H}|\Psi_T\rangle}{\langle\Psi_T|e^{-2\Theta H}|\Psi_T\rangle}. \tag{4}$$

The above equation is valid, provided that $\langle\Psi_T|\Psi_0\rangle\neq 0$ and O denotes an arbitrary observable.

To see how H relates to H_{KLM}, we compute the square in Eq. (3) to obtain

$$\begin{aligned}H=&\sum_{\vec{k},\sigma}\ \varepsilon(\vec{k})c^{\dagger}_{\vec{k},\sigma}c_{\vec{k},\sigma}+J\sum_{\vec{i}}\ \vec{S}^{c}_{\vec{i}}\cdot\vec{S}^{f}_{\vec{i}}\\&-\frac{J}{4}\sum_{\vec{i},\sigma}\ (c^{\dagger}_{\vec{i},\sigma}c^{\dagger}_{\vec{i},-\sigma}f_{\vec{i},-\sigma}f_{\vec{i},\sigma}+\text{H.c.})\\&+\frac{J}{4}\sum_{\vec{i}}\ (n^{c}_{\vec{i}}n^{f}_{\vec{i}}-n^{c}_{\vec{i}}-n^{f}_{\vec{i}}).\end{aligned} \tag{5}$$

As apparent, there are only pair-hopping processes between the f and c sites. Thus, the total number of doubly occupied and empty f sites is a conserved quantity:

$$\left[H,\sum_{\vec{i}}\ (1-n^{f}_{\vec{i},\uparrow})(1-n^{f}_{\vec{i},\downarrow})+n^{f}_{\vec{i},\uparrow}n^{f}_{\vec{i},\downarrow}\right]=0. \tag{6}$$

If we denote by Q_n the projection onto the Hilbert space with $\Sigma_{\vec{i}}(1-n^{f}_{\vec{i},\uparrow})(1-n^{f}_{\vec{i},\downarrow})+n^{f}_{\vec{i},\uparrow}n^{f}_{\vec{i},\downarrow}=n$ then

$$HQ_0=H_{KLM}+\frac{JN}{4}, \tag{7}$$

since in the Q_0 subspace the f sites are singly occupied and, hence, the pair-hopping term vanishes. Here, N corresponds to the number of unit cells. Thus, it suffices to choose

$$Q_0|\Psi_T\rangle=|\Psi_T\rangle, \tag{8}$$

to ensure that

$$\frac{\langle\Psi_T|e^{-\Theta H}Oe^{-\Theta H}|\Psi_T\rangle}{\langle\Psi_T|e^{-2\Theta H}|\Psi_T\rangle}=\frac{\langle\Psi_T|e^{-\Theta H_{KLM}}Oe^{-\Theta H_{KLM}}|\Psi_T\rangle}{\langle\Psi_T|e^{-2\Theta H_{KLM}}|\Psi_T\rangle}. \tag{9}$$

It is interesting to note that there is an alternative route to obtain the KLM. Instead of projecting onto the Q_0 Hilbert space, we can project onto the Q_N Hilbert space by suitably choosing the trial wave function,

$$\begin{aligned}HQ_N=&\sum_{\vec{k},\sigma}\ \varepsilon(\vec{k})c^{\dagger}_{\vec{k},\sigma}c_{\vec{k},\sigma}-\frac{J}{4}\sum_{\vec{i},\sigma}\ (c^{\dagger}_{\vec{i},\sigma}c^{\dagger}_{\vec{i},-\sigma}f_{\vec{i},-\sigma}f_{\vec{i},\sigma}+\text{H.c.})\\&+\frac{J}{4}\sum_{\vec{i}}\ (n^{c}_{\vec{i}}n^{f}_{\vec{i}}-n^{c}_{\vec{i}}-n^{f}_{\vec{i}}).\end{aligned} \tag{10}$$

Since in the Q_N subspace the f-sites are doubly occupied or empty, the exchange term $\vec{S}^{c}_{\vec{i}}\cdot\vec{S}^{f}_{\vec{i}}$ vanishes. To see the relation with the KLM, we define the spin-1/2 operators:

$$\tilde{S}^{+,f}_{\vec{i}}=-(-1)^{i_x+i_y}f^{\dagger}_{\vec{i},\uparrow}f^{\dagger}_{\vec{i},\downarrow},$$

$$\tilde{S}^{-,f}_{\vec{i}}=-(-1)^{i_x+i_y}f_{\vec{i},\downarrow}f_{\vec{i},\uparrow},\quad \tilde{S}^{z,f}_{\vec{i}}=\frac{1}{2}(n^{f}_{\vec{i}}-1), \tag{11}$$

which operate on the states: $|\Uparrow\rangle_{\vec{i},f}=-(-1)^{i_x+i_y}f^{\dagger}_{\vec{i},\uparrow}f^{\dagger}_{\vec{i},\downarrow}|0\rangle$ and $|\Downarrow\rangle_{\vec{i},f}=|0\rangle$ as well as the fermion operators:

$$\tilde{c}^{\dagger}_{\vec{i},\uparrow}=c^{\dagger}_{\vec{i},\uparrow},\quad \tilde{c}^{\dagger}_{\vec{i},\downarrow}=(-1)^{i_x+i_y}c_{\vec{i},\uparrow}. \tag{12}$$

With those definitions,

$$\begin{aligned}HQ_N=&\sum_{\vec{k},\sigma}\ \varepsilon(\vec{k})\tilde{c}^{\dagger}_{\vec{k},\sigma}\tilde{c}_{\vec{k},\sigma}+\frac{J}{2}\sum_{\vec{i}}\ (\tilde{S}^{+,c}_{\vec{i}}\tilde{S}^{-,f}_{\vec{i}}+\tilde{S}^{-,c}_{\vec{i}}\tilde{S}^{+,f}_{\vec{i}})\\&+J\tilde{S}^{z,c}_{\vec{i}}\tilde{S}^{z,f}_{\vec{i}}+\frac{JN}{4},\end{aligned} \tag{13}$$

which is nothing but the KLM.

A. Basic formalism

Having shown the relationship between H and H_{KLM} we now discuss some technical aspects of the QMC evaluation of $\langle\Psi_T|e^{-\Theta H}Oe^{-\Theta H}|\Psi_T\rangle/\langle\Psi_T|e^{-2\Theta H}|\Psi_T\rangle$. With the use of the Trotter formula we obtain

$$\langle\Psi_T|e^{-2\Theta H}|\Psi_T\rangle=\left\langle\Psi_T\left|\prod_{\tau=1}^{M}\ e^{\Delta\tau H_t}e^{-\Delta\tau H_J}\right|\Psi_T\right\rangle+\mathcal{O}(\Delta\tau^2). \tag{14}$$

Here, $H_t=-t\Sigma_{\langle\vec{i},\vec{j}\rangle,\sigma}c^{\dagger}_{\vec{i},\sigma}c_{\vec{j},\sigma}+\text{H.c.}$, $H_J=-J/4\Sigma_{\vec{i}}\vec{S}^{c}_{\vec{i}}\cdot\vec{S}^{f}_{\vec{i}}$, and $M\Delta\tau=2\Theta$. Strictly speaking, the systematic error produced by the above Trotter decomposition should be of order $\Delta\tau$. However, if the trial wave function, as well as H_t and H_J are simultaneously real representable, it can be shown that the prefactor of the linear $\Delta\tau$ error vanishes.[21,22]

Since we will ultimately want to integrate out the fermionic degrees of freedom, we carry out a Hubbard-Stratonovitch (HS) decomposition of the perfect square term:[23]

$$
\begin{aligned}
e^{-\Delta\tau H_J}&=\prod_{\vec{i}}\ e^{\Delta\tau J/4\{(\Sigma_\sigma c^{\dagger}_{\vec{i},\sigma}f_{\vec{i},\sigma}+\text{H.c.})^2\}},\\
&=\prod_{\vec{i}}\ \Bigg(\sum_{l=\pm1,\pm2}\ \gamma(l)e^{\sqrt{\Delta\tau J/4}\eta(l)\Sigma_\sigma c^{\dagger}_{\vec{i},\sigma}f_{\vec{i},\sigma}+\text{H.c.}}\\
&\quad+\mathcal{O}(\Delta\tau^4)\Bigg),
\end{aligned}
\tag{15}
$$

where the fields η and γ take the values:

$$
\gamma(\pm1)=1+\sqrt{6}/3,\quad \gamma(\pm2)=1-\sqrt{6}/3,
$$

$$
\eta(\pm1)=\pm\sqrt{2(3-\sqrt{6})},\quad \eta(\pm2)=\pm\sqrt{2(3+\sqrt{6})}.
$$

As indicated, this transformation is approximate and produces on each time slice a systematic error proportional to $\Delta\tau^4$. This amounts to a net systematic error of order $M\Delta\tau^4\sim2\Theta\Delta\tau^3$, which for constant values of the projection parameter, is an order smaller that the error produced by the Trotter decomposition.

The trial wave function is required to be a Slater determinant factorizable in the spin indices:

$$
|\Psi_T\rangle=|\Psi_T^{\uparrow}\rangle\otimes|\Psi_T^{\downarrow}\rangle,\quad \text{with}
$$

$$
|\Psi_T^{\sigma}\rangle=\prod_{y=1}^{N_\sigma}\Bigg(\sum_x\ a^{\dagger}_{x,\sigma}P^{\sigma}_{x,y}\Bigg)|0\rangle. \tag{16}
$$

Here, we have introduced the notation $x\equiv(\vec{i},n)$ where $\vec{i}$ denotes the unit cell and n the orbital (i.e., $a^{\dagger}_{(\vec{i},1),\sigma}=c^{\dagger}_{\vec{i},\sigma}$ and $a^{\dagger}_{(\vec{i},2),\sigma}=f^{\dagger}_{\vec{i},\sigma}$). It is convenient to generate $|\Psi_T^{\sigma}\rangle$ from a single particle Hamiltonian $H_0^{\sigma}=\Sigma_{x,y}a^{\dagger}_x(h_0^{\sigma})_{x,y}a_y$, which has the trial wave function as non-degenerate ground state. To obtain a trial wave function that satisfies the requirements $Q_0|\Psi_T\rangle=|\Psi_T\rangle$, we are forced to choose H_0 of the form:

$$
\begin{aligned}
H_0=&\sum_{\langle\vec{i},\vec{j}\rangle,\sigma}(t_{\vec{i},\vec{j}}c^{\dagger}_{\vec{i},\sigma}c_{\vec{j},\sigma}+\text{H.c.})\\
&+h_z\sum_{\vec{i}}\ e^{i\vec{Q}\cdot\vec{i}}(f^{\dagger}_{\vec{i},\uparrow}f_{\vec{j},\uparrow}-f^{\dagger}_{\vec{i},\downarrow}f_{\vec{j},\downarrow}),
\end{aligned}
\tag{17}
$$

which generates a Néel state $[\vec{Q}=(\pi,\pi)]$ on the localized orbitals. To obtain a non-degenerate ground state, we impose the dimerization

$$
t_{\vec{i},\vec{i}+\vec{a}_x}=\begin{cases}-t(1+\delta) & \text{if}\quad i_x=2n+1\\ -t(1-\delta) & \text{if}\quad i_x=2n\end{cases},
$$

$$
t_{\vec{i},\vec{i}+\vec{a}_y}=-t(1+\delta), \tag{18}
$$

with $\delta\ll t$.

We are now in a position to integrate out the fermionic degrees of freedom to obtain:

$$
\begin{aligned}
\langle\Psi_T|e^{-2\Theta H}|\Psi_T\rangle=&\sum_{\{l\}}\Bigg(\prod_{\vec{i},\tau}\ \gamma(l_{\vec{i},\tau})\Bigg)\\
&\times\prod_{\sigma}\ \det\Bigg(P^{\sigma\dagger}\prod_{\tau=1}^{M}\ e^{-\Delta\tau\hat{T}}e^{\hat{J}(\tau)}P^{\sigma}\Bigg),
\end{aligned}
\tag{19}
$$

where the matrices $\hat{T}$ and $\hat{J}(\tau)$ are defined via:

$$
H_t=\sum_{\vec{k},\sigma}\ \epsilon(\vec{k})c^{\dagger}_{\vec{k},\sigma}c_{\vec{k},\sigma}=\sum_{x,y,\sigma}\ a^{\dagger}_{x,\sigma}\hat{T}_{x,y}a_{y,\sigma},
$$

$$
\sum_{x,y,\sigma}\ a^{\dagger}_{x,\sigma}\hat{J}(\tau)_{x,y}a_{y,\sigma}.=\sqrt{\Delta\tau J/4}\sum_{\vec{i},\sigma}\ \eta(l_{\vec{i},\tau})(c^{\dagger}_{\vec{i},\sigma}f_{\vec{i},\sigma}+\text{H.c.}). \tag{20}
$$

The HS field l has acquired a space $\vec{i}$ and time τ index.

The basic ingredients to compute observables are equal-time Green functions. They are given by

$$
\begin{aligned}
&\frac{\langle\Psi_T|e^{-\Theta H}a_{x,\sigma}a^{\dagger}_{y,\sigma}e^{-\Theta H}|\Psi_T\rangle}{\langle\Psi_T|e^{-2\Theta H}|\Psi_T\rangle}\\
&=\sum_{\{l\}}\ \Pr(l)\langle\langle a_{x,\sigma}a^{\dagger}_{y,\sigma}\rangle\rangle(l),\quad \text{with}\\
&\langle\langle a_{x,\sigma}a^{\dagger}_{y,\sigma}\rangle\rangle(l)=[1-U^{>}_{\sigma,l}(U^{<}_{\sigma,l}U^{>}_{\sigma,l})^{-1}U^{<}_{\sigma,l}]_{x,y},\\
&U^{>}_{\sigma,l}=\prod_{\tau=1}^{M/2}\ e^{-\Delta\tau\hat{T}}e^{\hat{J}(\tau)}P^{\sigma}\\
&U^{<}_{\sigma,l}=P^{\sigma\dagger}\prod_{\tau=M}^{M/2+1}\ e^{-\Delta\tau\hat{T}}e^{\hat{J}(\tau)},\quad \text{and}\\
&\Pr(l)=\frac{\Big[\prod_{\vec{i},\tau}\ \gamma(l_{\vec{i},\tau})\Big]\prod_{\sigma}\ \det(U^{<}_{\sigma,l}U^{>}_{\sigma,l})}{\sum_{\{l\}}\Big[\prod_{\vec{i},\tau}\ \gamma(l_{\vec{i},\tau})\Big]\prod_{\sigma}\ \det(U^{<}_{\sigma,l}U^{>}_{\sigma,l})}.
\end{aligned}
\tag{21}
$$

Since, for a given set of HS fields, we are solving a free-electron problem interacting with an external field, a Wick theorem applies. Hence, from the knowledge of the the single-particle Green function at fixed HS configuration, we may evaluate all observables. Imgaginary time displaced correlation functions may equally be calculated.[24,25]

We are left with the summation over the HS fields, which we will carry out with Monte Carlo methods. In order to do

so without further complication, we have to be able to interpret $\Pr(l)$ as a probability distribution. This is possible only provided that $\Pr(l)\geqslant 0$ for all HS configurations. In the particle-hole symmetric case, the above statement is valid. Starting from the identity:

$$\det(U^{<}_{\uparrow,l}U^{>}_{\uparrow,l}) = \lim_{\beta\to\infty} \frac{\mathrm{Tr}\left(e^{-\beta H_0^{\uparrow}} \prod_{\tau=1}^{M} e^{-\Delta\tau H_t^{\uparrow}} e^{H_J^{\uparrow}(\tau)} \right)}{\mathrm{Tr}(e^{-\beta H_0^{\uparrow}})}, \tag{22}$$

we can carry out a particle-hole transformation

$$c^{\dagger}_{\vec{i},\uparrow} \to (-1)^{i_x+i_y} c_{\vec{i},\downarrow} \quad \text{and} \quad f^{\dagger}_{\vec{i},\uparrow} \to -(-1)^{i_x+i_y} f_{\vec{i},\downarrow}. \tag{23}$$

Here, $H_t^{\sigma}=\Sigma_{x,y} a^{\dagger}_{x,\sigma}\hat{T}_{x,y}a_{y,\sigma}$ and $H_J^{\sigma}(\tau) = \Sigma_{x,y} a^{\dagger}_{x,\sigma}\hat{J}(\tau)_{x,y}a_{y,\sigma}$. Since Eq. (23) corresponds to a canonical transformation, the trace remains invariant and $H_0^{\uparrow}$, $H_t^{\uparrow}$, as well as $H_J^{\uparrow}(\tau)$, map onto $H_0^{\downarrow}$, $H_t^{\downarrow}$, and $H_J^{\downarrow}(\tau)$, respectively. Thus, we have shown that: $\det(U^{<}_{\uparrow,l}U^{>}_{\uparrow,l}) = \det(U^{<}_{\downarrow,l}U^{>}_{\downarrow,l})$, which leads to $\Pr(l)\geqslant 0$ for all values of the HS fields. Away from half filling (which would correspond to adding a chemical potential term in H_0), particle hole-symmetry is broken and $\Pr(l)$ may become negative. This leads to the well-known sign problem. It is clear that by choosing $H_0^{\uparrow}=H_0^{\downarrow}$ thus leading to $P^{\uparrow}=P^{\downarrow}$ would produce positive values of $\Pr(l)$ for all HS configurations and irrespective of particle-hole symmetry. This stands in analogy to the absence of the sign problem in the attractive Hubbard model. However, this choice of the trial wave function is incompatible with the requirement $Q_0|\Psi_T\rangle=|\Psi_T\rangle$.

For the Monte Carlo sampling of the probability distribution $\Pr(l)$, we adopt a sequential single spin-flip algorithm. The details of the upgrading procedure, as well as of the numerical stabilization of the code, are similar to those used for auxiliary field QMC simulations of the Hubbard model.[26]

B. Optimizing the algorithm

The above straightforward approach for the QMC simulation of H turns out to be numerically inefficient. The major reason for this stems from the choice of the trial wave function. The coupled constraints (i) $Q_0|\Psi_T\rangle=|\Psi_T\rangle$ and (ii) $|\Psi_T\rangle$ is a Slater determinant factorizable in the spin indices make it impossible to choose a spin-singlet trial wave function (the trial wave function generated by the single particle Hamiltonian H_0 of Eq. (17) orders the f electrons in a Néel state that is not a spin singlet). Since we know that the ground state of the KLM on a finite-size system is a spin singlet,[27,28] we have to filter out all the spin excited states from the trial wave function to obtain the ground state. This is certainly not a problem when we are investigating the physics of a problem with a large spin gap, as is the case in the limit $J/t\gg 1$. However, in the limit of small J/t, the long-range magnetic order is present, and hence, one expects finite-size spin-gap to scale as v_s/L where v_s is the spin velocity and L the linear size of the system. In this case, starting with a spin-singlet trial wave function is important to obtain reliable convergence.[24]

In order to circumvent the above problem, we relax the constraint $Q_0|\Psi_T\rangle=|\Psi_T\rangle$ and add a Hubbard term for the f sites to the Hamiltonian.

$$H=\sum_{\vec{k},\sigma} \varepsilon(\vec{k}) c^{\dagger}_{\vec{k},\sigma}c_{\vec{k},\sigma} - \frac{J}{4}\sum_{\vec{i}} \left[\sum_{\sigma} c^{\dagger}_{\vec{i},\sigma}f_{\vec{i},\sigma} + f^{\dagger}_{\vec{i},\sigma}c_{\vec{i},\sigma} \right]^2 + U_f \sum_{\vec{i}} (n^f_{\vec{i},\uparrow}-1/2)(n^f_{\vec{i},\downarrow}-1/2). \tag{24}$$

This Hamiltonian is again block diagonal in the Q_n subspaces. During the imaginary time propagation, the components $Q_n|\Psi_T\rangle$ of the trial wave function will be suppressed by a factor $e^{-\Theta U_f n/2}$ in comparison to the component $Q_0|\Psi_T\rangle$.

The usual procedure to incorporate the Hubbard term in the QMC simulation relies on Hirsch's HS transformation:[29]

$$\exp\left[-\Delta\tau U \sum_{\vec{i}} \left(n^f_{\vec{i},\uparrow}-\frac{1}{2} \right)\left(n^f_{\vec{i},\downarrow}-\frac{1}{2} \right) \right] = \tilde{C} \sum_{s_1,\ldots,s_N=\pm 1} \exp\left[\tilde{\alpha}\sum_{\vec{i}} s_{\vec{i}}(n^f_{\vec{i},\uparrow}-n^f_{\vec{i},\downarrow}) \right], \tag{25}$$

where $\cosh(\tilde{\alpha})=\exp(\Delta\tau U/2)$. As apparent from the above equation, for a fixed set of HS fields, $s_1 \ldots s_N$, SU(2) spin symmetry is broken. Clearly SU(2) spin symmetry is restored after summation over the HS fields.

Alternatively, one may consider[29]

$$\exp\left[-\Delta\tau U \sum_{\vec{i}} \left(n_{\vec{i},\uparrow}-\frac{1}{2} \right)\left(n_{\vec{i},\downarrow}-\frac{1}{2} \right) \right] = C \sum_{s_1,\ldots,s_N=\pm 1} \exp\left[i\alpha\sum_{\vec{i}} s_{\vec{i}}(n_{\vec{i},\uparrow}+n_{\vec{i},\downarrow}-1) \right], \tag{26}$$

where $\cos(\alpha)=\exp(-\Delta\tau U/2)$ and $C=\exp(\Delta\tau UN/4)/2^N$. With this choice of the HS transformation, SU(2) spin invariance is retained for any given HS configuration. Even taking into account the overhead of working with complex numbers, one of the authors has argued[30] that this choice of HS transformation produces a more efficient code.

Having relaxed the condition $Q_0|\Psi_T\rangle=|\Psi_T\rangle$, we are now free to choose a spin singlet trial wave function that we generate from:

$$H_0=\sum_{\vec{k},\sigma} \varepsilon(\vec{k}) c^{\dagger}_{\vec{k},\sigma}c_{\vec{k},\sigma} - \frac{J}{4}\sum_{\vec{i},\sigma} (c^{\dagger}_{\vec{i},\sigma}f_{\vec{i},\sigma} + f^{\dagger}_{\vec{i},\sigma}c_{\vec{i},\sigma}), \tag{27}$$

which is nothing but the noninteracting PAM with hybridization $V=J/4$. The ground state at half filling is clearly a spin singlet. With this choice of the trial wave function, and the Hubbard-Stratonovitch transformation of Eq. (26), the

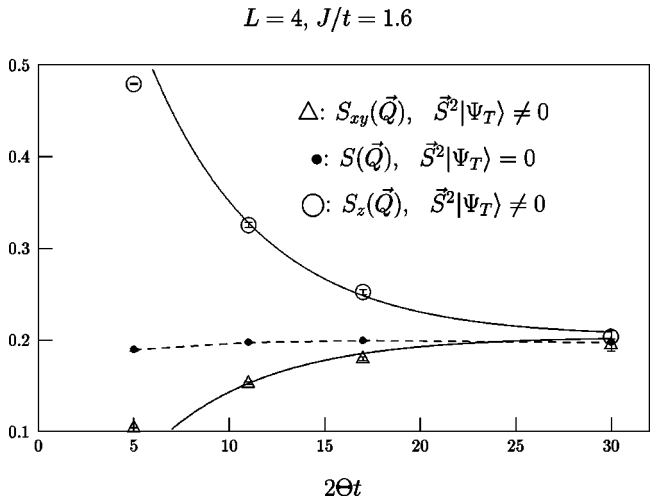

FIG. 1. Spin-spin correlations as a function of the projection parameter Θ. Here, $S(\vec{Q})=\frac{4}{3}\langle \vec{S}^f(\vec{Q})\cdot\vec{S}^f(-\vec{Q})\rangle$, $S^f_z(\vec{Q})=4\langle \vec{S}^f_z(\vec{Q})\cdot\vec{S}^f_z(-\vec{Q})\rangle$, and $S^f_{xy}(\vec{Q})=2(\langle \vec{S}^f_x(\vec{Q})\cdot\vec{S}^f_x(-\vec{Q})\rangle + \langle \vec{S}^f_y(\vec{Q})\cdot\vec{S}^f_y(-\vec{Q})\rangle)$. The trial wave function with $\vec{S}^2|\Psi_T\rangle\neq 0$ ($\vec{S}^2|\Psi_T\rangle=0$) corresponds to the ground state of the Hamiltonian in Eq. (27) [Eq. (17)]. In the *large* Θ limit, the results are independent on the choice of the trial wave function. In particular, starting from a broken-symmetry state the symmetry is restored at *large* values of Θt. For this system, the spin gap is given by $\Delta_{sp}=0.169\pm 0.004$ (Ref. 31). Starting with a trial wave function with $\vec{S}^2|\Psi_T\rangle\neq 0$, convergence to the ground state follows approximatively the form: $a+be^{-\Delta_{sp}2\Theta}$. The solid lines correspond to a least-square fit to this form.

particle-hole transformation of Eq. (23) maps $\det(U^{<}_{\uparrow,l,s}U^{>}_{\uparrow,l,s})$ on $\overline{\det(U^{<}_{\downarrow,l,s}U^{>}_{\downarrow,l,s})}$. Hence, no sign problem occurs at half filling.

Figure 1 demonstrates the importance of using a spin singlet trial wave function. Starting from a Néel order for the *f*- electrons, convergence to the ground state follows approximatively $e^{-\Delta_{sp}2\Theta}$, where Δ_{sp} corresponds to the spin gap. When the spin gap is small, convergence is poor and the remedy is to consider a spin singlet trial wave function.

Having optimized the trial wave function we now consider convergence as a function of J/t. As apparent from Fig. 2, for small values of J/t, increasingly large projection parameters are required to obtain convergence. The origin of this behavior may be traced back to the energy scale of the RKKY interaction that follows a J^2 law. At $J/t=0.4$, $2\Theta t \sim 40$ is enough to obtain convergence whereas at $J/t=0.2$, a value of $2\Theta t\sim 170$ is required.

The systematic error produced by the Trotter decomposition scales as $(\Delta\tau)^2$. This behavior is shown in Fig. 3. All our calculations were carried out at values of $\Delta\tau$ small enough so as to neglect this systematic error.

C. Ferromagnetic exchange

Until now, we have implicitly considered an antiferromagnetic exchange, $J>0$. It is straightforward to generalize the above case to a ferromagnetic one. The only point to take care of is the choice of the trial wave function in order to

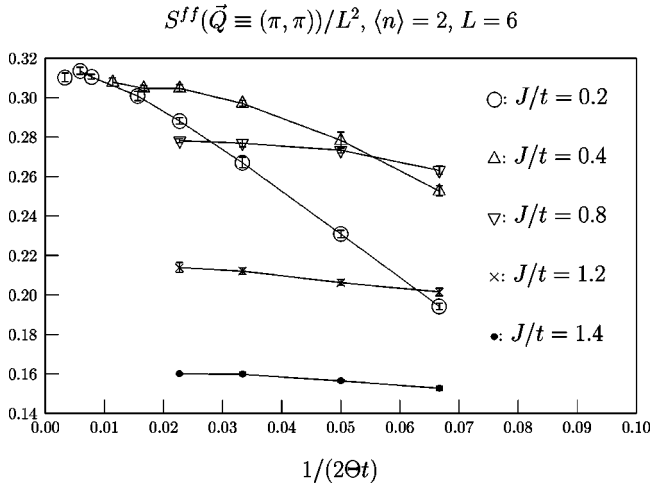

FIG. 2. Spin structure factor at $\vec{Q}=(\pi,\pi)$ for the *f* electrons $[S^{ff}(\vec{Q})]$ at various values of J/t and as a function of the projection parameter Θt. Here we consider a spin singlet trial wave function.

avoid the sign problem. In this case, the noninteracting Hamiltonian that generates the trial wave function has to be invariant under the particle-hole transformation:

$$c^{\dagger}_{\vec{i},\uparrow}\rightarrow(-1)^{i_x+i_y}c_{\vec{i},\downarrow} \quad \text{and} \quad f^{\dagger}_{\vec{i},\uparrow}\rightarrow+(-1)^{i_x+i_y}f_{\vec{i},\downarrow}. \tag{28}$$

Note that in comparison to Eq. (23), there is an overall sign difference in the particle-hole transformation of the *f* operators. With this condition one has: $\det(U^{<}_{\uparrow,l,s}U^{>}_{\uparrow,l,s}) = \overline{\det(U^{<}_{\downarrow,l,s}U^{>}_{\downarrow,l,s})}$ so that no sign problem occurs. The trial wave function is thus generated from the noninteracting Hamiltonian:

$$H_0=\sum_{\vec{k},\sigma}\varepsilon(\vec{k})c^{\dagger}_{\vec{k},\sigma}c_{\vec{k},\sigma}-\frac{J}{4}\sum_{\langle\vec{i},\vec{j}\rangle,\sigma}(c^{\dagger}_{\vec{i},\sigma}f_{\vec{j},\sigma}+f^{\dagger}_{\vec{j},\sigma}c_{\vec{i},\sigma}). \tag{29}$$

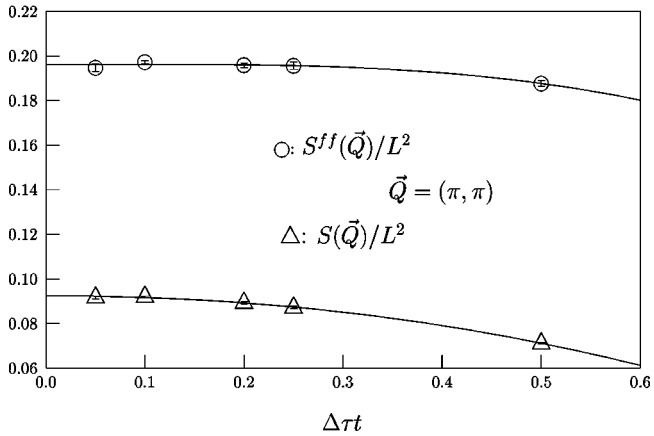

FIG. 3. Systematic error produce by the Trotter decomposition. In our simulations, we have used $\Delta\tau=0.1$ and $\Delta\tau=0.2$. Here, $S(\vec{Q})$ corresponds to the spin structure factor of the total spin at $\vec{Q}=(\pi,\pi)$.

D. Finite-temperature algorithm

The QMC method presented above may be generalized to finite temperatures to compute expectation values of observables in the grand-canonical ensemble:

$$\langle O\rangle = \frac{\mathrm{Tr}(e^{-\beta H}O)}{\mathrm{Tr}(e^{-\beta H})}. \tag{30}$$

Since the step from the $T=0$ approach to the finite-T algorithm is similar to the one for the standard Hubbard model, we refer the reader to the Ref. 26. We note however, that at finite temperatures, the projection onto the Q_0 subspace may only be achieved via the inclusion of the Hubbard term $U_f\Sigma_i(n^f_{i,\uparrow}-1/2)(n^f_{i,\downarrow}-1/2)$ in the Hamiltonian. At this point, it is very convenient to choose the SU(2) invariant HS decomposition of Eq. (26) since one can take the limit $U_f \to\infty$ by setting $\alpha=\pi/2$. Hence, irrespective of the considered temperature, we are guaranteed to be in the correct Hilbert space.

III. SPIN AND CHARGE DEGREES OF FREEDOM AT $T=0$

The different phases occurring at half filling are summarized in Fig. 4. All quantities have been extrapolated to the thermodynamic limit.[31] We have considered sizes ranging from 4×4 to 12×12 with periodic boundary conditions. The staggered moment

$$m_s = \lim_{L\to\infty}\sqrt{\frac{4}{3}\langle\vec{S}(\vec{Q})\cdot\vec{S}(-\vec{Q})\rangle}, \tag{31}$$

indicates the presence of long-range magnetic order. Here, $\vec{S}(\vec{Q})=(1/L)\Sigma_j e^{i\vec{Q}\cdot\vec{j}}\vec{S}(\vec{j})$ where $\vec{S}(\vec{j})=\vec{S}^f(\vec{j})+\vec{S}^c(\vec{j})$ is the total spin, $\vec{Q}=(\pi,\pi)$ the antiferromagnetic wave vector, and L corresponds to the linear size of the system. This quantity is maximal at $J/t=-\infty$ and vanishes at $J_c/t\sim1.45$, thus signaling a phase transition. The onset of a spin gap,

$$\Delta_{sp} = \lim_{L\to\infty} E_0^L(S=1,\ N_p=2N) - E_0^L(S=0,\ N_p=2N), \tag{32}$$

is observed when magnetic order disappears. Here, $E_0^L(S,N_p)$ is the ground-state energy on a square lattice with $N=L^2$ unit cells, N_p electrons, and spin S. Finally, the system remains an insulator for all considered coupling constants. This is supported by a nonvanishing quasiparticle gap,

$$\Delta_{qp} = \lim_{L\to\infty} E_0^L(S=1/2,\ N_p=2N+1) - E_0^L(S=0,\ N_p=2N). \tag{33}$$

We will first discuss the spin degrees of freedom and then turn our attention to charge degrees of freedom.

A. Spin degrees of freedom

To investigate the spin degrees of freedom, we compute the dynamical spin susceptibility,

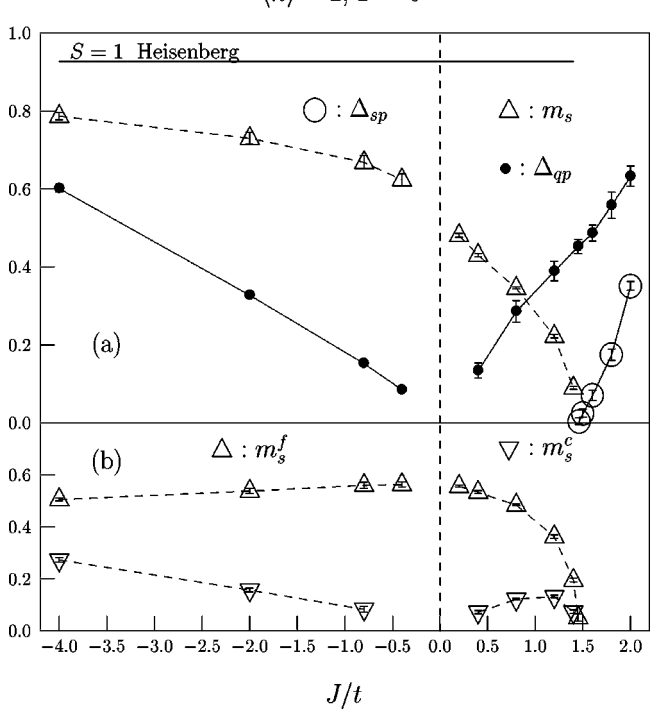

FIG. 4. (a) Staggered moment m_s, spin gap Δ_{sp}, and quasiparticle gap for the ferromagnetic and antiferromagnetic KLM. All quantities have been extrapolated to the thermodynamic limit based on results on lattice sizes up to 12×12. The data for $J>0$ stems from Ref. 31. The staggered moment corresponds to that of the total spin [see Eq. (31)]. The solid line corresponds to the value of the staggered moment for the $s=1$ antiferromagnetic model as obtained in a spin-wave approximation (Ref. 8). (b) Staggered moment of the f and c electrons after extrapolation to the thermodynamic limit.

$$S(\vec{q},\omega) = \pi\sum_n |\langle n|\vec{S}(\vec{q})|0\rangle|^2\delta[\omega-(E_n-E_0)], \tag{34}$$

where the sum runs over a complete set of eigenstates and $|0\rangle$ corresponds to the ground state. This quantity is related to the imaginary time spin-spin correlations that we compute with the QMC method:[31]

$$\langle 0|\vec{S}(\vec{q},\tau)\cdot\vec{S}(-\vec{q})|0\rangle = \frac{1}{\pi}\int d\omega e^{-\tau\omega}S(\vec{q},\omega). \tag{35}$$

Here, $\vec{S}(\vec{q},\tau)=e^{\tau H}\vec{S}(\vec{q})e^{-\tau H}$. We use the maximum entropy (ME) method to accomplish the above numerically ill-defined inverse Laplace transform.[18]

In the strong coupling limit $J\to\infty$, the model becomes trivial, since each f spin captures a conduction electron to form a singlet. In this limit, the ground state corresponds to a direct product of singlets on the f-c bonds of a unit cell. Starting from this state, one may create a magnon excitation by breaking a singlet to form a triplet. In second-order perturbation in t/J, this magnon acquires a dispersion relation given by

$$E_{sp}(\vec{q}) = J - \frac{16t^2}{3J} + \frac{4t^2}{J}\gamma(\vec{q}), \tag{36}$$

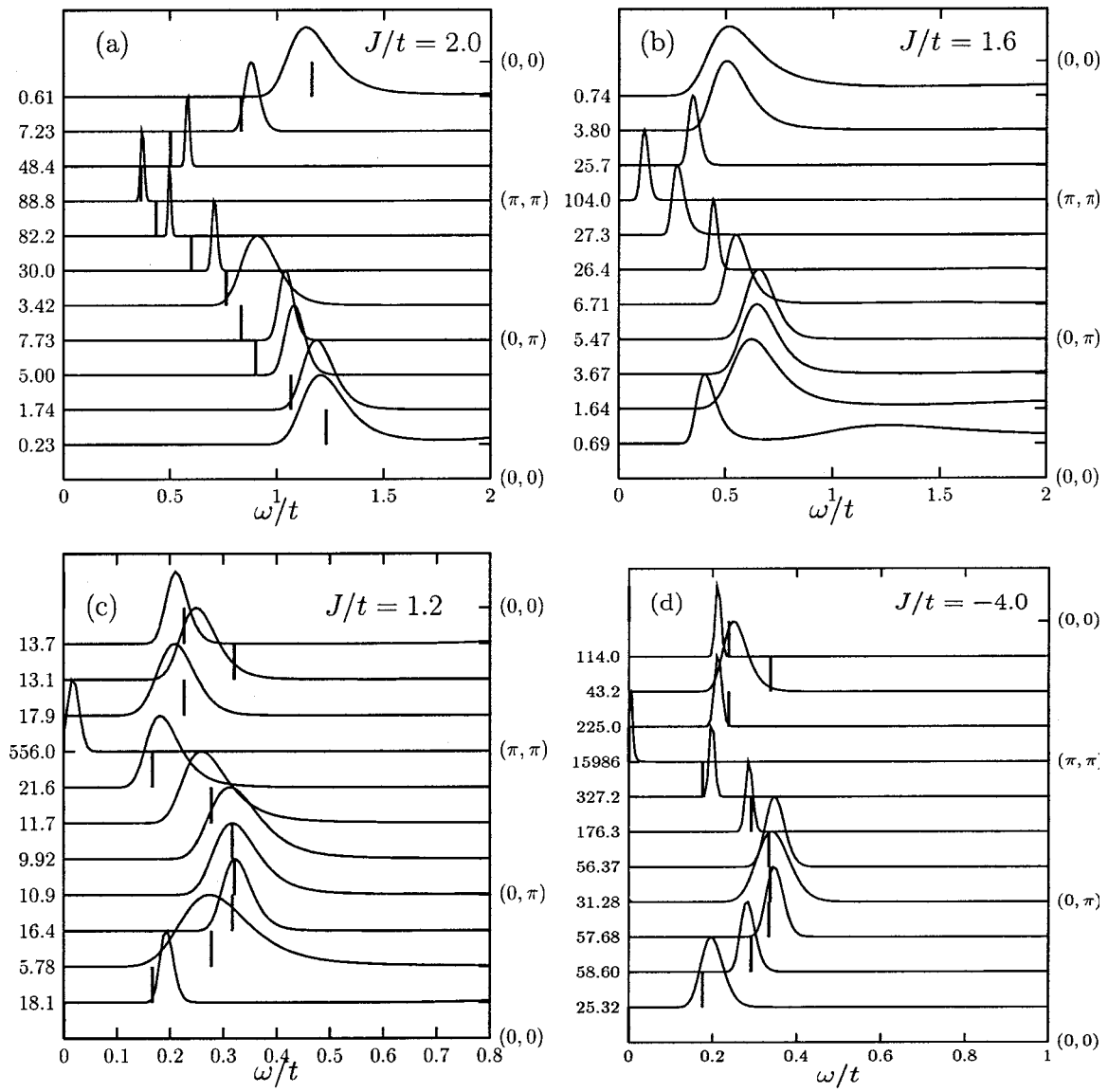

FIG. 5. Dynamical spin structure factor at $T=0$ for the ferromagnetic and antiferromagnetic KLM. We have normalized the peak heights to unity. The numbers on the left-hand side of the figures correspond to the normalization factor. The vertical bars are fits to the data, see text. Due to finite-size effects, the peak at $\vec{Q}=(\pi,\pi)$ in the antiferromagnetic phase ($J/t=1.2$ and $J/t=-4$) is shifted to finite frequencies.

where $\gamma(\vec{q})=\cos(q_x)+\cos(q_y)$.[15] At $\vec{Q}=(\pi,\pi)$, $E_{sp}(\vec{q})$ is minimal and is nothing but the spin gap. In Fig. 5(a), we plot the dynamical spin structure factor for $J/t=2.0$. The solid bars in the plot correspond to a fit to the above strong-coupling functional form: $a+b\,\gamma(\vec{q})$. As apparent, this functional form reproduces well the QMC data. We note that this magnon mode lies below the particle-hole continuum located at $2\Delta_{qp}$ (see Fig. 4).

As we approach the antiferromagnetically ordered phase, one expects that the above magnon mode evolves towards a spin-wave form:

$$E_{sw}(\vec{q})=\frac{J_{sp}}{2}\sqrt{1-\gamma(\vec{q})^2/4}. \tag{37}$$

As apparent from Fig. 5(b), as one approaches J_c the spin gap vanishes and the magnon mode softens around $\vec{q}=\vec{0}$. In the antiferromagnetic phase [see Fig. 5(c)] the data follow well the above spin-wave form.

In the limit of large ferromagnetic couplings, the model maps onto the $S=1$ antiferromagnetic Heisenberg model. At $J/t=-\infty$, the ground state is macroscopically degenerate since the *f-c* bonds are effectively decoupled and occupied by a triplet with arbitrary *z* component of spin. This degeneracy is lifted in second-order perturbation theory, yielding a $S=1$ antiferromagnetic Heisenberg model:

$$H_{eff}=\frac{2t^2}{J}\sum_{\langle\vec{i},\vec{j}\rangle}\vec{\mathcal{S}}_{\vec{i}}\cdot\vec{\mathcal{S}}_{\vec{j}}. \tag{38}$$

Here, $\vec{\mathcal{S}}_{\vec{i}}=\Sigma_{m,m'}t^{\dagger}_{\vec{i},m}\vec{\sigma}^{(1)}_{m,m'}t_{\vec{i},m'}$, $t_{\vec{i},1}=c^{\dagger}_{\vec{i},\uparrow}f^{\dagger}_{\vec{i},\uparrow}$, $t_{\vec{i},0}=1/\sqrt{2}(c^{\dagger}_{\vec{i},\uparrow}f^{\dagger}_{\vec{i},\downarrow}+c^{\dagger}_{\vec{i},\downarrow}f^{\dagger}_{\vec{i},\uparrow})$, and $t_{\vec{i},-1}=c^{\dagger}_{\vec{i},\downarrow}f^{\dagger}_{\vec{i},\downarrow}$. $\vec{\sigma}^{(1)}$ correspond to the $s=1$ Pauli spin matrices. The magnetic excita-

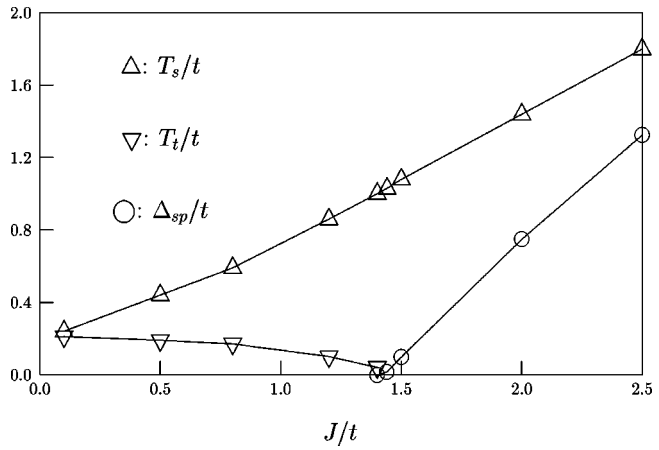

FIG. 6. Mean field of the two-dimensional Kondo necklace model. T_s (T_t) corresponds to the energy scale below that the bond singlets (triplets) condense. Δ_{sp} denotes the spin gap.

tions are clearly spin waves as confirmed by the QMC data of Fig. 5(d). In the limit of large negative J, the staggered moment should scale to the value obtained for the $S=1$ Heisenberg model. Within a spin-density wave approximation,[8] this quantity takes the value 0.93. As apparent from Fig. 4, the QMC data approaches smoothly this value as J/t decreases.

The quantum phase transition in the spin degrees of freedom at $J_c/t \sim 1.45$ may be described in the framework of the Kondo necklace model given by

$$H_{KN}=t\sum_{\vec{i},\vec{j}}\ (S_{\vec{i}}^{c,x}S_{\vec{j}}^{c,x}+S_{\vec{i}}^{c,y}S_{\vec{j}}^{c,y})+J\sum_{\vec{i}}\ \vec{S}_{\vec{i}}^{c}\cdot\vec{S}_{\vec{i}}^{f}. \qquad (39)$$

This model neglects charge fluctuations, and the spin-flip processes between conduction electrons mimic the kinetic energy. Although the Kondo necklace model has a lower symmetry [U(1)] than the KLM [SU(2)] one may expect this model to give a reasonable description of the spin degrees of freedom at energy scales smaller than the charge gap. A mean-field solution is obtained in terms of bond singlet and triplet operators.[32] Both the conduction and impurity spins are represented by singlets, $\Delta_{\vec{i}}^{\dagger}$, and triplets $\vec{t}_{\vec{i}}$ on the *f-c* bonds of the unit cell. The bond operators obey bosonic commutation rules and are subject to the constraint $\Delta_{\vec{i}}^{\dagger}\Delta_{\vec{i}}+\vec{t}_{\vec{i}}\vec{t}_{\vec{i}}=1$. At the mean-field level and generalizing the work of Zhang *et al.*[33] to finite temperatures, one obtains the phase diagram shown in Fig. 6. The condensation of singlets $s=\langle\Delta_{\vec{i}}^{\dagger}\rangle>0$ occurs at a temperature scale T_s, which, to a first approximation, tracks J. At $J>J_c$, the triplet excitations remain gapped and have a dispersion relation given by: $\omega(\vec{q})=\alpha\sqrt{1+s^2t\gamma(\vec{q})/\alpha}$ with $\alpha=s^2t(1+\sqrt{1+\Delta_{sp}^2/t^2s^2})$. Here, Δ_{sp} corresponds to the spin gap plotted in Fig. 6. The gap in the magnon spectrum at $\vec{q}=(\pi,\pi)\equiv\vec{Q}$ vanishes at $J_c/t \sim 1.4$ in remarkable agreement with the QMC results. We note that this mean-field approach shows no phase transition in the one-dimensional case consistently with numerical calculations.[15,33] For $J<J_c$, the ground state has both condensation of singlets ($s>0$) and of triplets at the antiferromagnetic wave vector ($\bar{t}=\sqrt{N}\langle t_{\vec{Q}}^{\dagger,x}\rangle>0$). The energy scale below which the triplet excitations condense is denoted by T_t in Fig. 6. In terms of the KLM, the condensation of triplets (singlets) follows from the RKKY interaction (Kondo effect). Thus, the fact that at the mean-field level, both s and $\bar{t}$ do not vanish may be interpreted as the coexistence of Kondo screening and antiferromagnetism in the ordered phase. We will confirm this point of view in the study of the charge degrees of freedom.

B. Charge degrees of freedom: the single-particle spectral function

To study the charge degrees of freedom, we compute the spectral function $A(\vec{k},\omega)$ which is related to the imaginary time Green function via:

$$\langle c_{\vec{k}}^{\dagger}(\tau)c_{\vec{k}}\rangle=\frac{1}{\pi}\int_0^{\infty}d\omega e^{-\tau\omega}A(\vec{k},-\omega). \qquad (40)$$

The Maximum Entropy (ME) method is used to extract $A(\vec{k},\omega)$. Starting from the bond-singlet ground state valid in the strong coupling limit, one can create a quasiparticle excitation, which to first order in t/J has the dispersion relation

$$E_{qp}(\vec{k})=3J/4+t\gamma(\vec{k}). \qquad (41)$$

$E_{qp}(\vec{k})$ is a minimal at $\vec{k}=(\pi,\pi)$ so that the quasiparticle gap takes the value $\Delta_{qp}=E_{qp}[\vec{k}=(\pi,\pi)]$. Comparison with Eq. (36) leads to $\Delta_c=2\Delta_{qp}>\Delta_{sp}$ in the strong-coupling limit. This marks the difference to a standard band insulator that satisfies $\Delta_c=\Delta_{sp}$. In accordance with the strong-coupling limit, the numerical data of Figs. 7(a)–(c) show that irrespective of J/t, the quasiparticle gap is defined by the $\vec{k}=(\pi,\pi)$ wave vector. Furthermore, comparison with Fig. 5 shows that the inequality $\Delta_c>\Delta_{sp}$ is valid for all considered coupling constants.

For antiferromagnetic couplings ($J>0$), the spectral function shows similar features in the ordered ($J<J_c$) and disordered ($J>J_c$) magnetic phases, thus lending support that Kondo screening, which is responsible for the functional form of the dispersion relation at strong couplings, is equally present in the ordered phase. However, upon closer analysis, shadow features are seen in the antiferromagnetically ordered phase. Shadows are most easily understood by considering the self-energy $\Sigma(\vec{k},\omega_m)\propto g^2/N\beta\Sigma_{\nu_m,\vec{q}}\chi(\vec{q},\nu_m)G_0(\vec{k}-\vec{q},\omega_m-\nu_m)$ describing electrons with propagator $G_0(\vec{k},\omega_m)$ scattering off spin fluctuations with coupling constant g. Long-range magnetic order at wave vector $\vec{Q}=(\pi,\pi)$ and staggered moment m_s justify the Ansatz $\chi(\vec{q},\nu_m)\propto m_s^2N\beta\delta_{\nu_m,0}\delta_{\vec{q},\vec{Q}}$ for the spin susceptibility. The Green function is then given by: $G(\vec{k},\omega_m)=1/[G_0^{-1}(\vec{k},\omega_m)-\alpha G_0(\vec{k}+\vec{Q},\omega_m)]$ with $\alpha\propto(gm_s)^2$. It is then easy to see that if $G(\vec{k},\omega)$ has a pole at ω_0 then $G(\vec{k}+\vec{Q},\omega)$ also has a pole at ω_0, i.e., the shadow. Numerically, it is convenient to establish the existence of shadows by considering the imaginary time Green function. Figure 8 plots $\langle c_{\vec{k}}^{\dagger}(\tau)c_{\vec{k}}\rangle$ for k

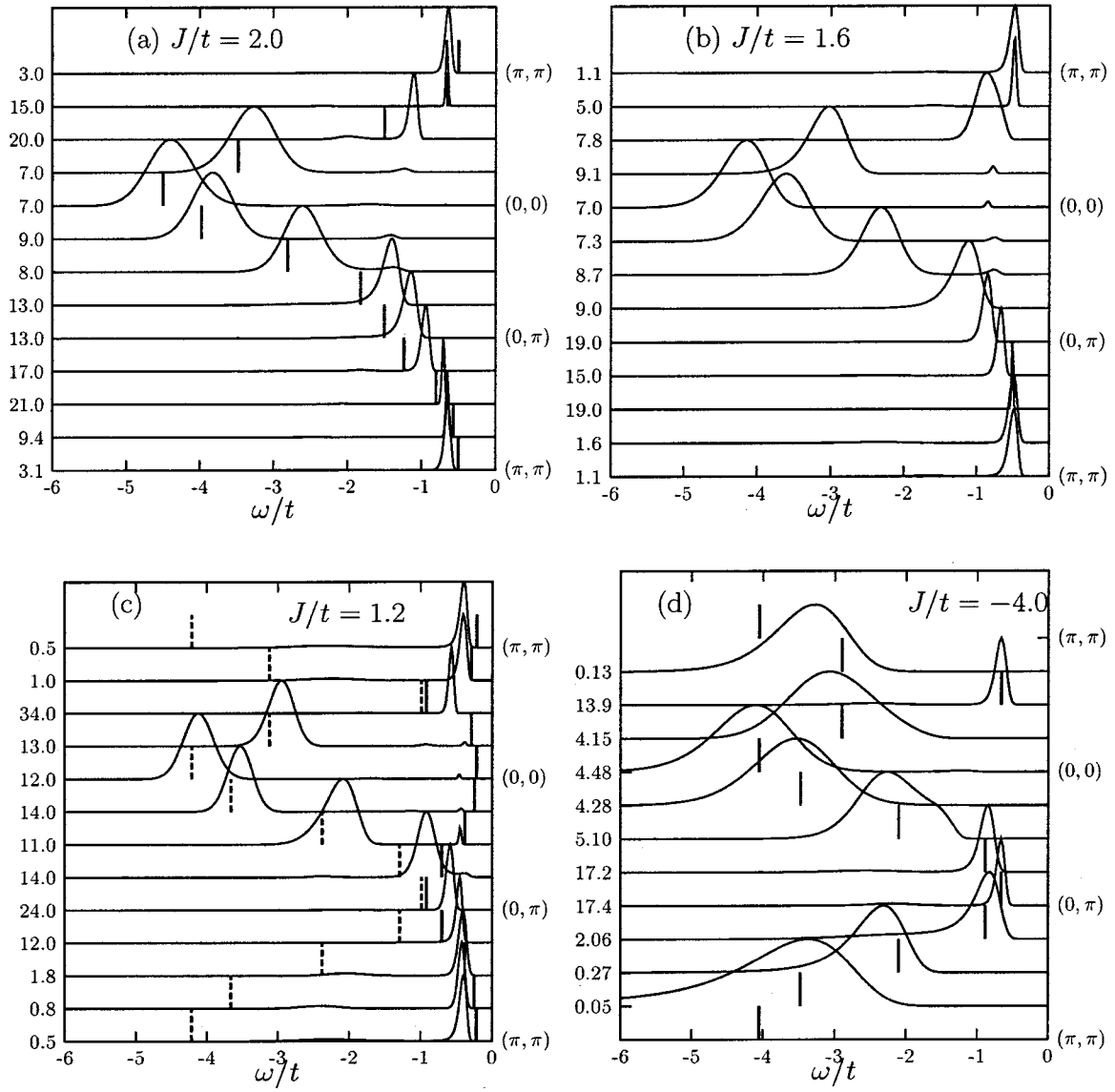

FIG. 7. Single-particle spectral function at $T=0$ for the ferromagnetic and antiferromagnetic KLM. We have normalized the peak heights to unity. The numbers on the left-hand side of the figures correspond to the normalization factor. The vertical bars are fits to the data, see text.

$=(\pi,\pi)$. At large values of τt this quantity follows an exponential law $e^{-\tau\Delta_{qp}}$. This exponential decay generates the pole in $A(\vec{k},\omega)$ at $\omega=-\Delta_{qp}$ [see Eq. (40)]. As argued above, due to the long-range antiferromagnetic order one expects a pole in $A(\vec{k}+\vec{Q},\omega)$ at $\omega=-\Delta_{qp}$, i.e., the shadow. As demonstrated in Fig. 8, $\langle c^{\dagger}_{\vec{k}+\vec{Q}}(\tau)c_{\vec{k}+\vec{Q}}\rangle$ shows the same asymptotic behavior as $\langle c^{\dagger}_{\vec{k}}(\tau)c_{\vec{k}}\rangle$. Thus, the low-energy feature around $\vec{k}=(0,0)$ in Fig. 7(c) corresponds to the shadow of the band in the vicinity of $\vec{k}=(\pi,\pi)$. We note that shadow features at high energies are hard to resolve within the ME. Close to the phase transition in the disordered phase precursors features of the shadow bands are seen [see Fig. 7(b)]. As is apparent, they are shifted by an energy scale that corresponds approximately to the spin gap.

To obtain further insight into the charge degrees of freedom we will consider a mean-field theory of the KLM recently introduced by Zhang and Yu.[34] This mean-field theory is appealing since (i) it takes into account both Kondo screening and magnetic ordering of the *f* and *c* electrons and (ii) a phase where both Kondo screening and magnetic ordering emerges in a narrow region around the phase transition.

Following Zhang and Yu,[34] we write the KLM as

$$
\begin{aligned}
H_{KLM}=&\sum_{\vec{k},\sigma}\varepsilon(\vec{k})c^{\dagger}_{\vec{k},\sigma}c_{\vec{k},\sigma}\\
&+\frac{J}{4}\sum_{\vec{i}}(f^{\dagger}_{\vec{i},\uparrow}f_{\vec{i},\uparrow}-f^{\dagger}_{\vec{i},\downarrow}f_{\vec{i},\downarrow})(c^{\dagger}_{\vec{i},\uparrow}c_{\vec{i},\uparrow}-c^{\dagger}_{\vec{i},\downarrow}c_{\vec{i},\downarrow})\\
&-\frac{J}{4}\sum_{\vec{i}}[(f^{\dagger}_{\vec{i},\downarrow}c_{\vec{i},\downarrow}+c^{\dagger}_{\vec{i},\uparrow}f_{\vec{i},\uparrow})^2\\
&+(f^{\dagger}_{\vec{i},\uparrow}c_{\vec{i},\uparrow}+c^{\dagger}_{\vec{i},\downarrow}f_{\vec{i},\downarrow})^2],
\end{aligned}
\tag{42}
$$

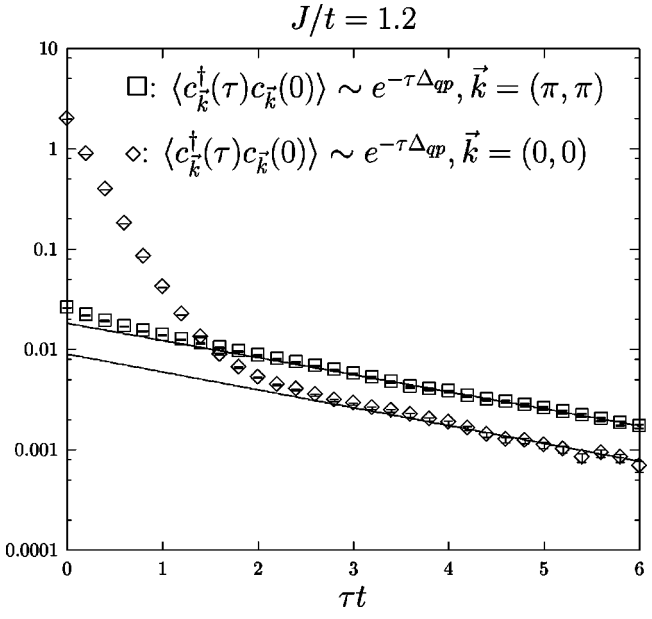

FIG. 8. $\langle c^\dagger_{\vec{k}+\vec{Q}}(\tau) c_{\vec{k}+\vec{Q}}\rangle$ and $\langle c^\dagger_{\vec{k}}(\tau) c_{\vec{k}}\rangle$ as a function of τt on a 8×8 lattice at $T=0$. Both considered $\vec{k}$ points follow a $e^{-\Delta_{qp}\tau}$ law (solid lines), thus confirming the existence of shadows.

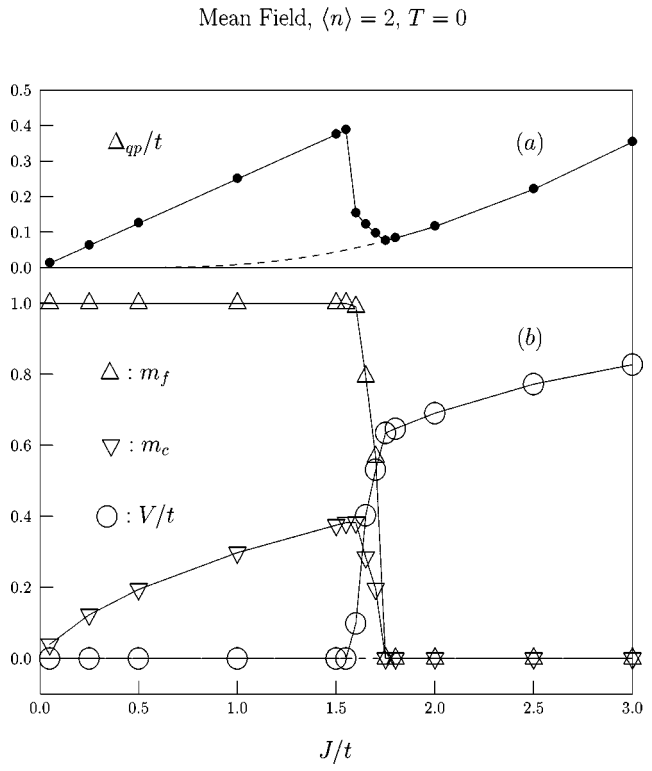

FIG. 9. Solution of the mean-field equations in Eq. (46). The solid line in (a) corresponds to the quasiparticle gap as obtained with the mean-field order parameters plotted in (b). The dashed line corresponds to the quasiparticle gap obtained in the absence of magnetic ordering (i.e., we consider the solution of the mean-field equations with $m_c, m_f = 0$ but $V \neq 0$. In the weak-coupling limit, those solutions produce higher energy values than when magnetic ordering is allowed.)

with the constraint: $f^\dagger_{\vec{i},\uparrow} f_{\vec{i},\uparrow} + f^\dagger_{\vec{i},\downarrow} f_{\vec{i},\downarrow} = 1$. The second term of Eq. (42) describes the polarization of the conduction electrons by the impurity spins and leads to a magnetic instability. The third term term is nothing but a rewriting of the spin-flip processes:

$$\frac{J}{2}\sum_{\vec{i}} (f^\dagger_{\vec{i},\uparrow} f_{\vec{i},\downarrow} c^\dagger_{\vec{i},\downarrow} c_{\vec{i},\uparrow} + f^\dagger_{\vec{i},\downarrow} f_{\vec{i},\uparrow} c^\dagger_{\vec{i},\uparrow} c_{\vec{i},\downarrow}), \tag{43}$$

which are at the origin of the screening of the impurity spins by the conduction electrons. The mean-field approximation proposed by Zhang and Yu[34] is based on the order parameters:

$$\langle f^\dagger_{\vec{i},\uparrow} f_{\vec{i},\uparrow} - f^\dagger_{\vec{i},\downarrow} f_{\vec{i},\downarrow}\rangle = m_f e^{i\vec{Q}\cdot\vec{i}},$$

$$\langle c^\dagger_{\vec{i},\uparrow} c_{\vec{i},\uparrow} - c^\dagger_{\vec{i},\downarrow} c_{\vec{i},\downarrow}\rangle = -m_c e^{i\vec{Q}\cdot\vec{i}} \quad \text{and}$$

$$\langle f^\dagger_{\vec{i},\downarrow} c_{\vec{i},\downarrow} + c^\dagger_{\vec{i},\uparrow} f_{\vec{i},\uparrow}\rangle = \langle f^\dagger_{\vec{i},\uparrow} c_{\vec{i},\uparrow} + c^\dagger_{\vec{i},\downarrow} f_{\vec{i},\downarrow}\rangle = -V. \tag{44}$$

Here, $\vec{Q}$ is the antiferromagnetic wave vector, m_f and m_c are, respectively, the staggered moments of the impurity spins and conduction electrons, and V is the hybridization order parameter that leads to the screening of the impurity spins. With the above Ansatz, one obtains the mean field Hamiltonian:

$$\tilde{H} = \sum_{\vec{k},\sigma} \begin{pmatrix} c_{\vec{k},\sigma} \\ c_{\vec{k}+\vec{Q},\sigma} \\ f_{\vec{k},\sigma} \\ f_{\vec{k}+\vec{Q},\sigma} \end{pmatrix}^\dagger \times \begin{pmatrix} \varepsilon(\vec{k}) & \frac{Jm_f\sigma}{4} & \frac{JV}{2} & 0 \\ \frac{Jm_f\sigma}{4} & -\varepsilon(\vec{k}) & 0 & \frac{JV}{2} \\ \frac{JV}{2} & 0 & 0 & -\frac{Jm_c\sigma}{4} \\ 0 & \frac{JV}{2} & -\frac{Jm_c\sigma}{4} & 0 \end{pmatrix} \times \begin{pmatrix} c_{\vec{k},\sigma} \\ c_{\vec{k}+\vec{Q},\sigma} \\ f_{\vec{k},\sigma} \\ f_{\vec{k}+\vec{Q},\sigma} \end{pmatrix} + NJ(m_f m_c/4 + V^2/2), \tag{45}$$

where the $\vec{k}$ sum runs over the magnetic Brillouin zone. We note that due to particle-hole symmetry present in the half filled case, the constraint of no double occupancy of the f sites is satisfied on average: $\langle f^\dagger_{\vec{i},\uparrow} f_{\vec{i},\uparrow} + f^\dagger_{\vec{i},\downarrow} f_{\vec{i},\downarrow}\rangle = 1$. The saddle point equations,

$$\left\langle \frac{\partial \tilde{H}}{\partial m_f} \right\rangle = \left\langle \frac{\partial \tilde{H}}{\partial m_c} \right\rangle = \left\langle \frac{\partial \tilde{H}}{\partial V} \right\rangle = 0, \tag{46}$$

may then be solved.[34]

Solutions to the saddle-point equations at $T=0$ and as a function of J/t are plotted in Fig. 9. As is apparent, solutions with $m_c, m_f \neq 0$, $V=0$, as well as with $m_c, m_f = 0$, $V \neq 0$ and most interestingly with $m_c, m_f, V \neq 0$ are obtained. Each solution predicts very different functional forms for the quasiparticle dispersion relation of the conduction electrons. Thus, by comparing with the numerical data, we can deduce which values of the mean-field order parameters are appropriate to best describe each phase.

We start by considering the spin-gap phase with $J > J_c$. Here, magnetic order is absent and the impurity spins are completely screened by the conduction electrons. It is thus appropriate to set $m_c = m_f = 0$ but $V \neq 0$. This yields two quasiparticle bands with dispersion relation:

$$E_{\pm}(\vec{k}) = \frac{1}{2}(\varepsilon(\vec{k}) \pm E(\vec{k})), \quad \text{with} \quad E(\vec{k}) = \sqrt{\varepsilon(\vec{k})^2 + (JV)^2}. \tag{47}$$

The quasiparticle weights are given by the coherence factors: $u_{\pm}(\vec{k})^2 = \frac{1}{2}[1 \pm \varepsilon(\vec{k})/E(\vec{k})]$. We can use this form to fit the QMC data shown in Fig. 7(a). As is apparent, the functional form of the dispersion relation is well reproduced.

We now consider $J < J_c$. Here, antiferromagnetic order is present both in the conduction electrons and localized spins so that: $m_c \neq 0$ as well as $m_f \neq 0$. Following the idea that the spin degrees of freedom are frozen due to the magnetic ordering, we set $V=0$ to obtain

$$E_{\pm}(\vec{k}) = \pm E(\vec{k}), \quad \text{with} \quad E(\vec{k}) = \sqrt{\varepsilon(\vec{k})^2 + (Jm_f/4)^2}. \tag{48}$$

The residues of the poles of the Green function follow: $u_{\pm}(\vec{k})^2 = \frac{1}{2}[1 \pm \varepsilon(\vec{k})/E(\vec{k})]$. This clearly does not reproduce the QMC results since the very flat quasiparticle band observed numerically around $\vec{k} = (\pi, \pi)$ is absent [see Fig. 7(c)]. Assuming, on the other hand, that magnetic ordering and Kondo screening coexist, we set $V \neq 0$ to obtain four quasiparticle bands:

$$E_{\pm,\pm}(\vec{k}) = \pm\frac{1}{\sqrt{2}}\left\{ E(\vec{k}) \pm \sqrt{E(\vec{k})^2 - \frac{J^4}{4}(m_c m_f/4 + V^2)^2 - J^2 m_c^2/4\varepsilon(\vec{k})^2} \right\}^{1/2}, \quad \text{with}$$

$$E(\vec{k}) = \varepsilon(\vec{k})^2 + J^2(m_c^2/4 + m_f^2/4 + 2V^2)/4. \tag{49}$$

An acceptable account of the numerical data is obtained by using the QMC values of the staggered moments and V as a fit parameter [see Fig. 7(c)]. We are thus led to the interpretation that the localized spins play a dual role. On one hand, they are partially screened by the conduction electrons. On the other hand, the remnant magnetic moment orders due to the RKKY interaction.

It is now interesting to consider the ferromagnetic KLM. When $J<0$, Kondo screening is not present. Thus, we expect the appropriate mean-field solution to have $m_c \neq 0$, as well as $m_f \neq 0$ but $V=0$. This choice of mean-field parameters leads to the dispersion relation given in Eq. (48). As apparent, and using m_f as a fit parameter, we can reproduce the QMC results [see Fig. 7(d)].

IV. SPIN AND CHARGE DEGREES OF FREEDOM AT FINITE TEMPERATURE

The aim of this section is to define relevant energy scales for both spin and charge degrees of freedom as a function of J/t. In doing so, we will discuss the behavior of the optical conductivity, staggered spin susceptibility, single particle spectral functions, as well as the specific heat as a function of temperature. We will put the emphasis on the behavior of those quantities at the spin and charge energy scales.

A. Spin and charge energy scales

To define the charge scale, we consider the charge susceptibility $\chi_c = \beta/L^2(\langle N^2\rangle - \langle N\rangle^2)$, where N corresponds to the particle number operator. It suffices to consider only the conduction electrons since the f electrons are localized and have no charge fluctuations. Since we are discussing the temperature dependence of χ_c, let us recall the high-temperature result:

$$\chi_c = \frac{1}{2T}\left[1 - \frac{1}{8T^2}\left(\frac{3J^2}{8} + 8t^2\right)\right]. \tag{50}$$

From that behavior, it appears that $J\chi_c$ will exhibit some approximative scaling form as a function of T/J only for large $J/t \gg 8/\sqrt{3} \sim 4.62$. In Fig. 10, we find consistent results at high temperature with Eq (50).

We can define a characteristic charge temperature T_C in a precise way by looking at the maximum of χ_c. In the weak-coupling limit, our numerical results are consistent with $T_C \sim J$ (See Figs. 10 and 19). In the large J limit ($J >$ bandwidth), the physics becomes local and one can consider decoupled sites. For each site, there are only eight states to take into account for computing the grand-canonical partition function: the singlet state, the threefold degenerate triplet, the fourfold degenerate $S=1/2$ state containing either an

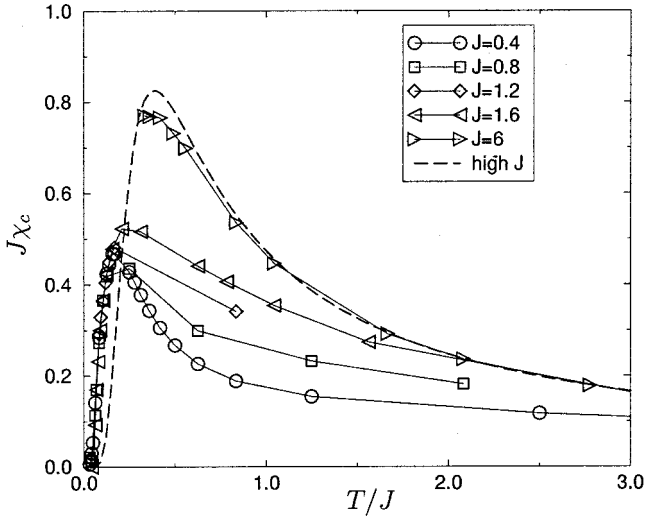

FIG. 10. Charge susceptibility $J\chi_c$ vs T/J for various couplings on the $L=6$ lattice. For very large J, we obtain good agreement with the large-J expression (51) plotted with a dashed line.

empty conduction site or a doubly occupied one, and with the two different spin configurations. In this limit, $\Delta_{sp}=J$, $\Delta_{qp}/J=3/4$, and

$$\chi_c=\beta\frac{4}{4+3e^{-\beta J/4}+e^{3\beta J/4}}, \tag{51}$$

which exhibits a peak at $T_C=0.386J$. Hence, and apart from different numerical prefactors at weak and strong couplings, T_C scales as J in both limits (see Fig. 19).

To best understand the meaning of the charge scale, we consider the real part of the optical conductivity as obtained from the Kubo formula, $\sigma(\omega,T)$. This quantity is related to the imaginary time current-current correlation functions via:

$$\langle J(\tau)J(0)\rangle=\int d\omega K(\omega,\tau)\sigma(\omega,T), \quad \text{with}$$

$$K(\omega,\tau)=\frac{1}{\pi}\frac{e^{-\tau\omega}\omega}{1-e^{-\beta\omega}}. \tag{52}$$

Here, J is the current operator along the x or y lattice direction and $\langle\rangle$ represents an average over the finite-temperature ensemble. The above inverse Laplace transform, to obtain the optical conductivity is carried out with the ME (Ref. 18) method. The default model is chosen as follows. We start at high temperature with a flat default and then, for lower temperatures, we take as default the result obtained at the temperature just above.[35] This allows us to obtain smoother results, but emphasizes the fact that the ME method depends on the default that is used.

The overall features of the conductivity are shown in Fig. 11 for a given J. At high temperatures, there is only a very broad lorentzian Drude peak. By lowering the temperature, we first observe an enhancement of the Drude weight as expected for a metal. At temperature scales lower than T_C, there is a transfer of spectral weight from the Drude peak to finite frequencies and finally, at very low temperatures, we observe the opening of an optical gap related to the quasiparticle gap observed in the single-particle density of states (DOS).

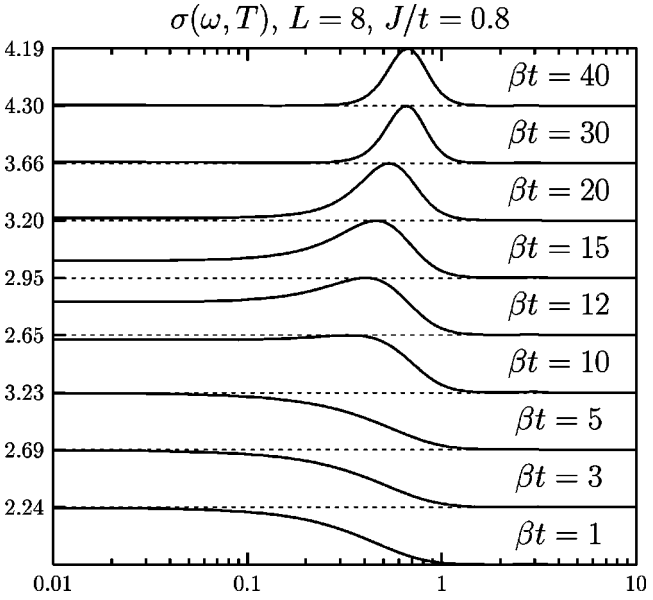

FIG. 11. Optical conductivity $\sigma(\omega,T)$ versus ω on a logarithmic scale for $J/t=0.8$ and various temperatures ($\Delta\tau=0.2$, $L=8$ lattice). The peak height has been normalized to unity and the normalization factor is listed on the left-hand side of the figure. As the temperature is decreased below the charge scale $T_C/t\sim0.16$ spectral weight is transferred from the Drude peak to finite frequencies.

The resistivity is defined as $\rho(T)=1/\sigma(0,T)$. In Fig. 12, we plot $\rho(T)$ for various J. We observe a minimum located at approximately T_C. Thus, we will conclude that T_C corresponds to an energy scale where scattering of the electrons is enhanced, while decreasing temperature due to the screening of magnetic impurities.

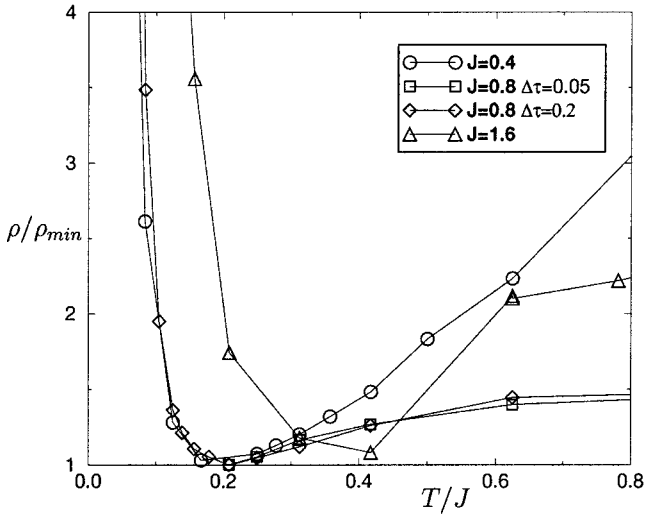

FIG. 12. Normalized dc resistivity ρ as a function of T/J for various couplings. We have checked for $J/t=0.8$ that the results do not depend on $\Delta\tau$. To a first approximation, and taking into account the scatter of the data at $J/t=1.6$, the temperature of the minimum in ρ tracks T_C: $T_C/J\sim0.2,0.2,0.25$ for $J/t=0.4$, 0.8, and 1.6, respectively.

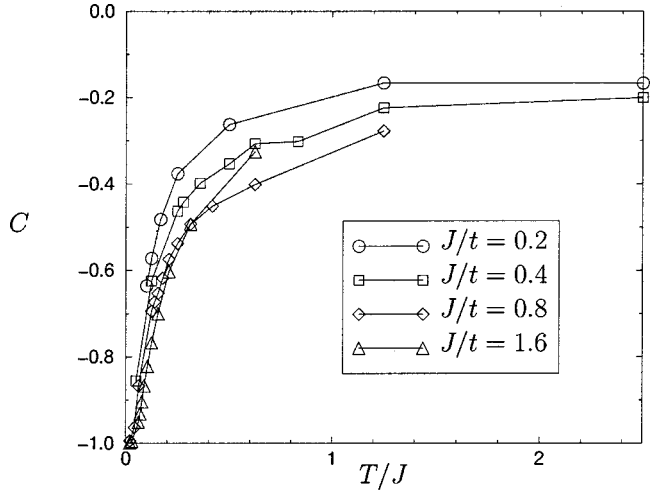

FIG. 13. Normalized local spin-spin correlation function $C=\langle \vec{S}_f\cdot\vec{S}_c\rangle(T)/|\langle \vec{S}_f\cdot\vec{S}_c\rangle(T=0)|$ as a function of T/J for various couplings. To a first approximation, the temperature scale of the onset of correlations tracks J.

This scenario is reinforced by the behavior of the local spin-spin correlation function $C=\langle \vec{S}_f\cdot\vec{S}_c\rangle(T)/|\langle \vec{S}_f\cdot\vec{S}_c\rangle(T=0)|$ plotted in Fig. 13. As the temperature is lowered, this quantity decreases indicating the formation of local singlets. Since the curves are almost identical as a function of T/J and for various couplings, we deduce that the typical energy scale is J and that the formation of those singlets are responsible for the enhancement of the resistivity which occurs at a similar temperature.

Before considering the characteristic energy scale for the spin degrees of freedom, we comment on the relation between the optical gap—as obtained from the low-temperature conductivity data—and quasiparticle gap (see Sec. III). They are not directly related since optical transitions involve only zero-momentum transfer. Starting from the hybridization picture, we can represent the band structure as in Fig. 14.

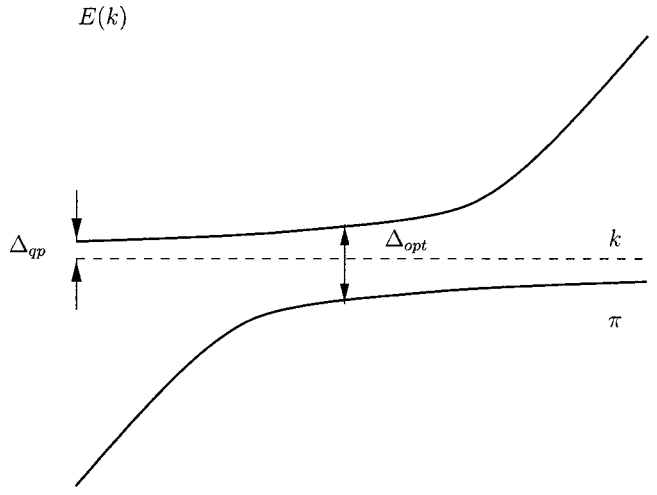

FIG. 14. Schematic 1D band structure showing the hybridized bands. k varies for $k=0$ to $k=\pi$ and as apparent charge gap $\Delta_C \sim 2\Delta_{qp}$ is smaller than the optical gap Δ_{opt}.

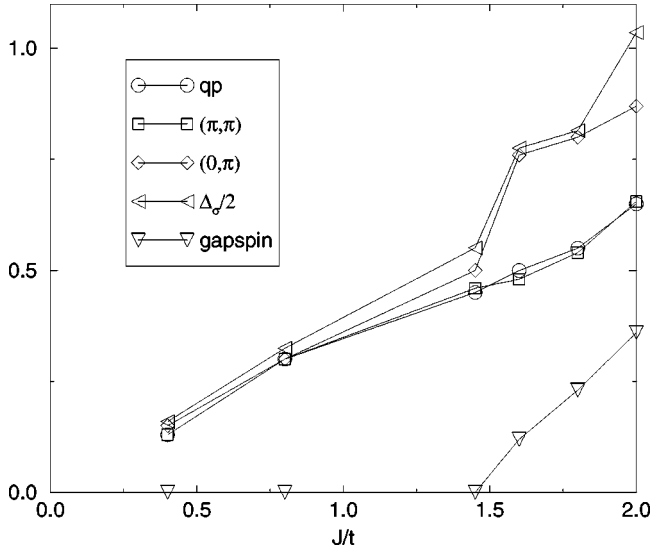

FIG. 15. Various gaps as a function of J. We have considered low enough temperatures so as to reproduce ground-state results and $L=6$. The quasiparticle gap is obtained from the DOS, the gaps at (π,π) and (0,0) are seen in the spectral functions at those points, the optical gap, Δ_σ stems from the optical conductivity and finally, the spin gap Δ_{sp} is taken from Ref. 31. As apparent, in the weak-coupling limit, where the quasiparticle dispersion is very flat along the $\vec{k}=(\pi,\pi)$ to $\vec{k}=(0,\pi)$ direction, the optical and charge gaps are comparable (see Fig. 7).

Generalizing this figure to 2D, we clearly see that the smallest optical gap is at $\vec{k}=(\pi,0)$ (or equivalent points) and is larger than the charge gap $\Delta_c \simeq 2\Delta_{qp}$. We recall that the quasiparticle gap corresponds to a transfer from a particle at $k=(\pi,\pi)$ in the lower band to the chemical potential. We then expect from that naive argument $\Delta_{opt}>\Delta_C \simeq 2\Delta_{qp}$. More precisely, we can relate the optical gap to the gap at $\vec{k}=(0,\pi)$ as observed in Fig. 15.

To define a characteristic energy for the spin degrees of freedom, we compute the uniform spin susceptibility, $\chi_s=\beta/L^2(\langle m_z^2\rangle-\langle m_z\rangle^2)$. Here, $m_z=\Sigma_{\vec{i}}(n_{\vec{i},\uparrow}-n_{\vec{i},\downarrow})$ with $n_{\vec{i},\sigma}=c^\dagger_{\vec{i},\sigma}c_{\vec{i},\sigma}+f^\dagger_{\vec{i},\sigma}f_{\vec{i},\sigma}$. In order to observe magnetic properties, it can be necessary to go to very low temperatures when J is small. With our algorithm, which is free from the sign problem, we can go down to $T=0.01t$ for $L=6$ or $T=0.02t$ for $L=8$.

In a high-temperature expansion, χ_s takes the form:

$$\chi_s=\frac{3}{8T}\left(1-\frac{J}{6T}\right). \tag{53}$$

From this expansion, one expects to observe a scaling property $J\chi_s=f(T/J)$ in this regime. This is indeed what is observed in Fig. 16 for $T/J\geqslant 0.6$. We define the magnetic characteristic temperature T_S via the position of the maximum in χ_s. At large coupling, the physic of the Kondo lattice becomes local. In that limit, the susceptibility is easily computed [see a similar calculation for the charge susceptibility in Eq. (51)] and takes the form:

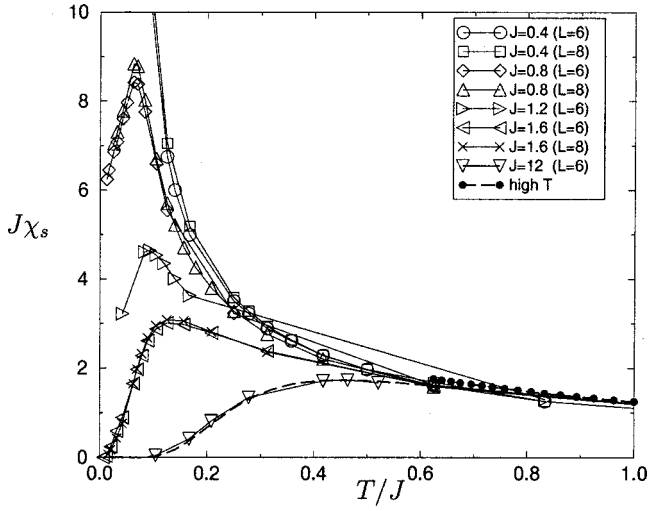

FIG. 16. Uniform spin susceptibility $J\chi_s$ as a function of T/J for various couplings and lattice sizes. The high-temperature expansion (53) is shown with filled circles and the large-coupling expansion (54) is plotted in dashed line.

$$\chi_s = \beta \frac{1+2e^{-\beta J/4}}{4+3e^{-\beta J/4}+e^{3\beta J/4}}, \tag{54}$$

which exhibits a maximum at $T_S \simeq 0.453J$. In contrast, for smaller J, the position of the maximum clearly increases more slowly than J (see Fig. 17). As is apparent from Fig. 17 and for the considered values of J/t, T_S scales approximately as J^2.

Figure 19 plots T_S as a function of J. In the large coupling region, we have excellent agreement with the expansion of Eq. (54); but, for couplings up to ~ 5 (or bandwidth, which is the physical case), T_S is well fitted by $\sim J^2$.

The meaning of the energy scale T_S is elucidated by considering the spin susceptibility at the antiferromagnetic wave vector $\vec{Q}=(\pi,\pi)$. This quantity measures the antiferromagnetic correlation length. Indeed, writing the spin-spin correlation functions in space and imaginary time as $S(\vec{r},\tau) = A\exp(i\vec{r}\cdot\vec{Q})\exp(-r/\xi)\exp(-\tau/\xi_\tau)$, we find that the staggered susceptibility $\chi_s(\vec{Q}) = \int_o^\beta d\tau \int d\vec{r}\exp(-i\vec{Q}\cdot\vec{r})S(\vec{r},\tau) \sim \xi^D \xi_\tau$ in D dimensions. For the Heisenberg model, the dynamical exponent z defined by $\xi_\tau \sim \xi^z$ is equal to 1.[36,37] Since the charge degrees of freedom are gapped, we expect that our model is in the same universality class as the O(3) model. We then obtain in our case $\chi_s(\vec{Q}) \sim \xi^3$.

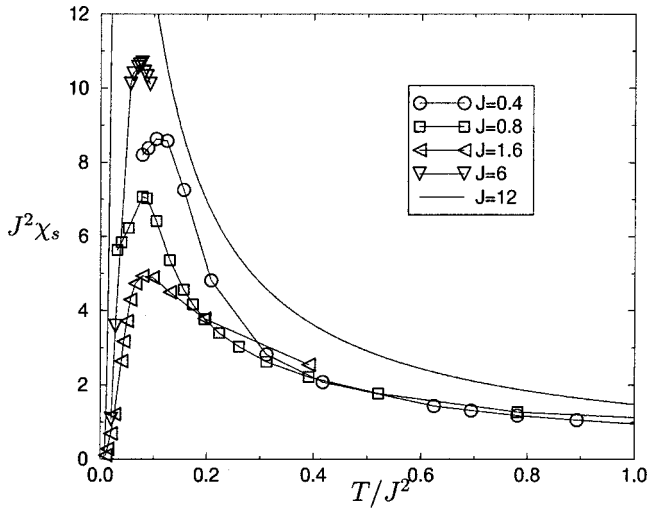

FIG. 17. Uniform spin susceptibility $J^2\chi_s$ as a function of T/J^2 for various couplings and $L=8$. For $J \leqslant 6$, the maximum T_S/J^2 is roughly constant.

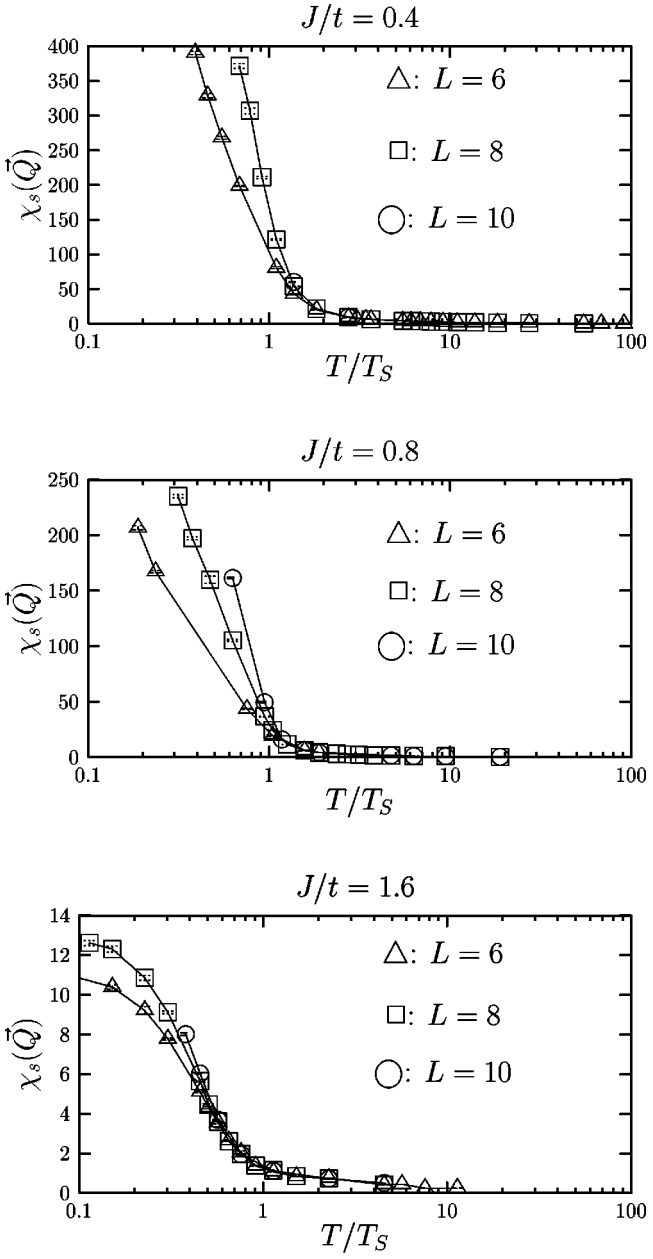

FIG. 18. Staggered spin susceptibility $\chi_s(\vec{Q})$ for various couplings and sizes. Since $\chi_s(\vec{Q}) \sim \xi^3$, we can extract the behavior of the antiferromagnetic correlation length ξ. $T_S \simeq 0.017, 0.05, 0.22$ for $J/t = 0.4, 0.8, 1.6$.

$\chi_s(\vec{Q})$ is plotted in Fig. 18. As apparent and for the considered J/t range, the energy scale T_S marks the onset of

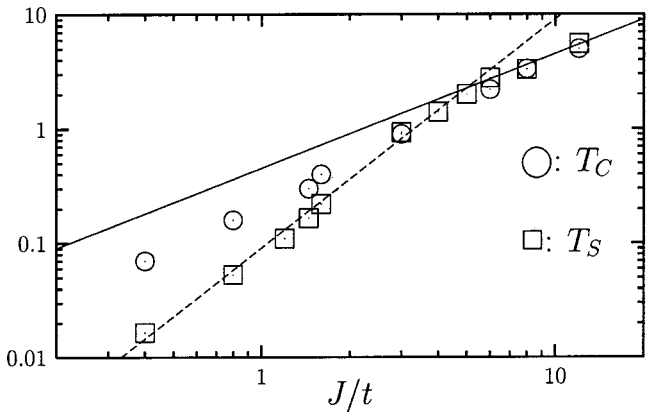

FIG. 19. Characteristic spin T_S and charge T_C temperatures as defined by the maximum of χ_s and χ_c as a function of J for $L=6$ and $L=8$ when available. At large J, the asymptotic behavior of T_S is $0.453J$ [Eq. (54) shown in full line] with no adjustable parameter; at small J, T_S is well fitted by the form $J^2/11$ (dashed line).

short-range antiferromagnetic fluctuations. At low temperatures in the ordered phase, one expects ξ to grow exponentially as a function of decreasing temperature. On the other hand, in the spin-gap phase, $J/t>1.45$, the antiferromagnetic correlation length saturates to a constant.[37]

The results of this section are summarized in Fig. 19. We have defined both a charge, T_C and a spin T_S scales. The charge scale corresponds to the onset of enhanced scattering as a function of decreasing temperature due to the screening of the magnetic impurities. Apart from different numerical prefactors T_C scales as J in the weak- and strong-coupling limits. From weak to intermediate couplings, the spin scale defines the onset of short-range antiferromagnetic fluctuations and follows a J^2 law in agreement with the energy scale associated to the RKKY interaction. At strong couplings, T_S tracks the spin gap. We note that we find good agreement with exact diagonalizations studies at finite temperatures.[38] This approach is, however, limited to very small cluster sizes and consequently to high temperatures and/or large values of J/t where the local approximation becomes valid. Thus, those studies cannot extract the behavior of T_S in the weak coupling limit.

B. Temperature dependence of spectral functions and origin of quasiparticle gap

The origin of the quasiparticle gap in the strong-coupling limit is the formation of Kondo singlets. In the weak-coupling limit, the situation is not *a priori* clear. In the mean-field theory presented in Fig. 9, and retaining only Kondo screening, we obtain an exponentially small gap corresponding to the dashed line in Fig. 9(a). On the other hand, retaining only magnetic ordering, the quasiparticle gap takes the value $J/4t$ in good agreement with the numerical data. We note that an exponentially small gap is equally obtained with (i) Gutzwiller approximation;[12] (ii) dynamical mean-field theory;[10] (iii) $1/N$ expansion[39] since those approximations neglect magnetic fluctuations. In this section, we argue that at or slightly below T_C a small gap emerges leading to the

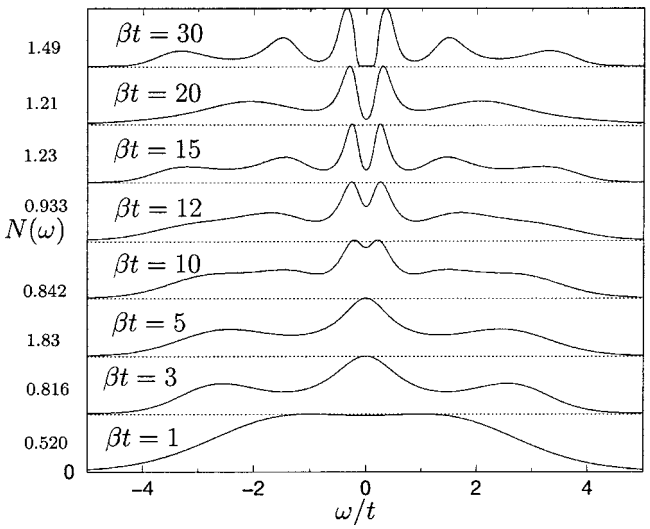

FIG. 20. Integrated DOS for $J/t=0.8$ on the $L=8$ lattice for various temperatures shown on the plot. The peak height is normalized to unity and normalization factor is listed on the left-hand side of the figure.

quasiparticle dispersion relation $\frac{1}{2}(\varepsilon(\vec{k})\pm\sqrt{\varepsilon^2(\vec{k})+\Delta^2})/2$ and that the quasiparticle gap of order J is formed only at T_S.

We start by considering the integrated DOS, $N(\omega)$ obtained with the ME method. Results are shown in Fig. 20 at $J/t=0.8$. In the vicinity of the charge scale, $T_C=0.16t$, one observes a reduction of spectral weight at the Fermi energy. Within the mean-field approximation of the KLM presented in Eqs. (42) and (44), this dip in the DOS of the conduction electrons follows directly from the occurrence of Kondo screening, i.e., $V\neq 0$. Hence, this feature in $N(\omega)$ at T_C stands in agreement with our interpretation of the charge scale T_C. As the temperature is lowered below T_C, the density of states at the Fermi level is further depleted and a gap opens in the low temperature limit.

In order to gain more insight into the distribution of spectral weight, it is convenient to compute the momentum-dependent DOS, $A(\vec{k},\omega)$. The integrated density of states merely corresponds to the sum over all $\vec{k}$ of $A(\vec{k},\omega)$. Therefore, we expect the same behavior by decreasing the temperature but we have more information on the dispersion relations of the excitations for example. Fig. 21(a) plots $A(\vec{k},\omega)$ again for $J/t=0.8$ and at a temperature $T=0.083t$ corresponding to $T_S<T<T_C$. For comparison, we have included the $T=0$ data [see Fig. 21(b)]. As apparent the substantial spectral weight of the $\vec{k}$ points on the non-interacting Fermi line, i.e., $\vec{k}=(0,\pi),(\pi/2,\pi/2)$ has shifted to lower energies. This is the origin of the decrease in spectral weight observed at the Fermi level in the integrated DOS at $T\simeq T_C$. However, the flat dispersion relation around $\vec{k}=(\pi,\pi)$—with significantly less spectral weight—remains pinned at the Fermi level. The dominant features of the quasiparticle dispersion relation are well reproduced by the fit: $(\varepsilon(\vec{k})\pm\sqrt{\varepsilon^2(\vec{k})+\Delta^2})/2$ with $\Delta=0.5t$. This value of Δ produces a quasiparticle gap $\Delta_{qp}=\Delta^2/16t\simeq 0.016t$ that lies be-

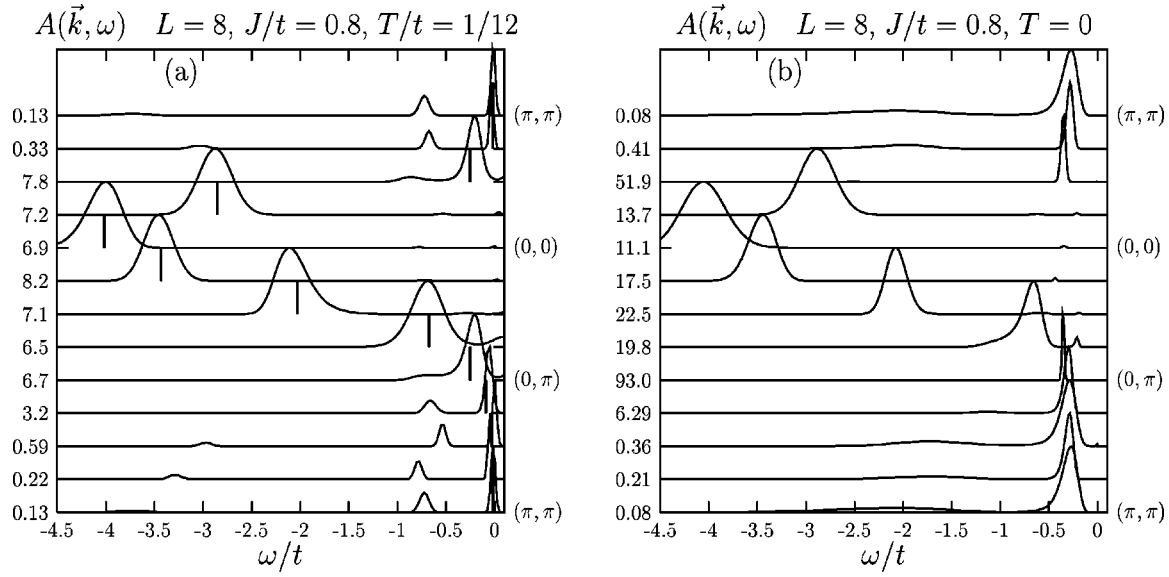

FIG. 21. (a) Spectral functions for $J/t=0.8$ and $\beta t=12$ ($\Delta\tau=0.2$, $L=8$ lattice). Normalization factors are written on the vertical axis. At this temperature, $T_S<T<T_C=0.2t$, there is a clear formation of hybridized bands with quasiparticle gap lying beyond our resolution. The vertical bars correspond to a fit of the data (see text). For comparison, we have included the $T=0$ results (b).

yond our resolution. As seen in Fig. 21(b), $\Delta_{qp}=0.28\pm0.02$ in the zero-temperature limit.

Since the quasiparticle gap is determined by the $\vec{k}=(\pi,\pi)$ wave vector we concentrate on this k point to analyze the temperature evolution. As is apparent in Fig. 22 at $J/t=0.8$, the quasiparticle gap of order J is formed approximately at the magnetic scale $T_S=0.05t$. Since the model is particle-hole symmetric $A(\vec{k},\omega)=A(\vec{k}+\vec{Q},-\omega)$. Thus, the fact that the peak splits symmetrically around the Fermi energy confirms the presence of shadow bands. In the spin-gap phase, the quasiparticle gap originates solely from Kondo screening. In the mean-field approximation presented in Eqs. (42) and (44) and retaining only Kondo screening, the quasiparticle gap will grow continuously as a function of decreasing temperatures below the charge scale. This merely reflects the temperature dependence of the mean-field order parameter V. Precisely this behavior is seen in Fig. 22 at $J/t=1.6$.

The evolution of the quasiparticle gap as a function of temperature is equally seen in the charge susceptibility. At low temperatures one expects $\chi_c=\beta\exp(-\Delta_{qp}\beta)$. As is apparent from Fig. 23, it is only below T_S that the data follows the above exponential form.

C. Specific heat

Finally, we consider the specific heat that contains information on both spin and charge degrees of freedom. In principle, one can obtain the specific heat $C_v(T)$ by direct cal-

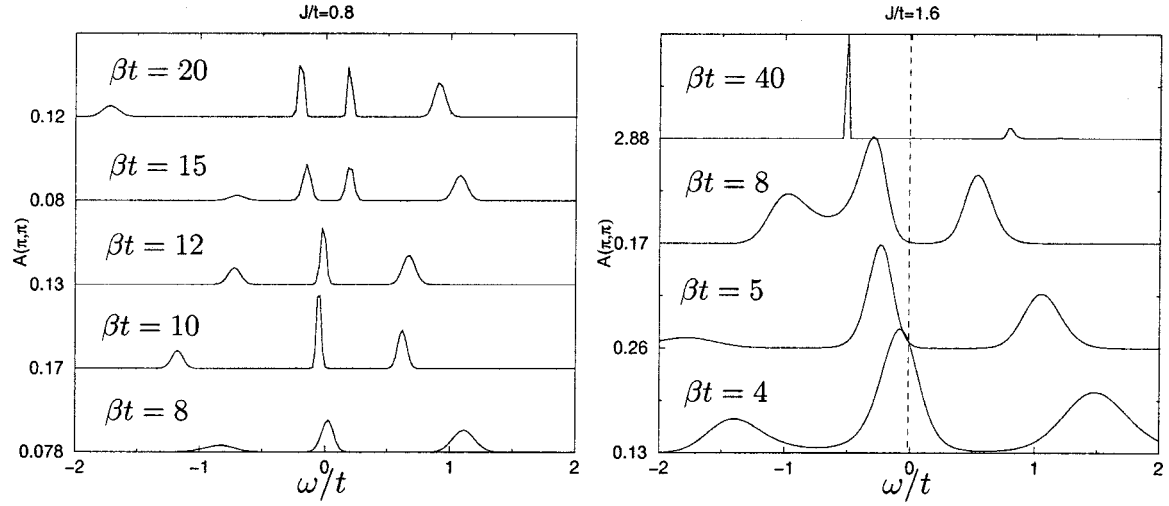

FIG. 22. Spectral functions at (π,π) for various couplings and β (increasing from down to up) ($\Delta\tau=0.2$, $L=8$ lattice). At $J/t=0.8$, the quasiparticle gap of order $J/4t$ opens at a temperature scale comparable to $T_S=0.05$. In the spin-gap phase, at $J/t=1.6$ the quasiparticle gap grows smoothly as a function of decreasing temperature.

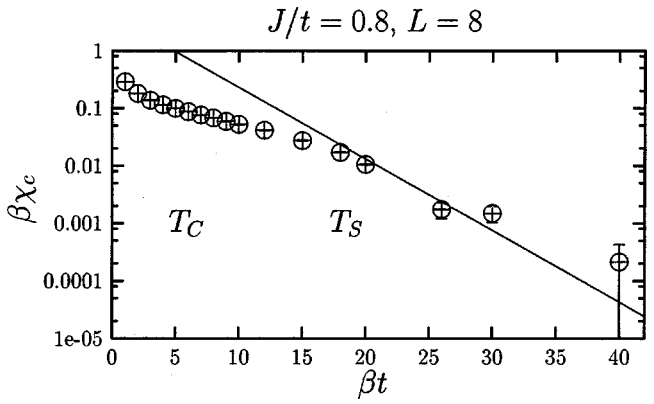

FIG. 23. χ_c/β at $J/t=0.8$. The solid line corresponds to $\exp(-\Delta_{qp}\beta)$ where quasiparticle corresponds to the value obtained with $T=0$ simulations (See Fig. 4). Only below the spin scale, T_S, do the data follow the above exponential form.

culation of the fluctuations of the internal energy $E(T)$: $C_v(T)=1/NdE/dT=1/N(\langle H^2\rangle-\langle H\rangle^2)/T^2$. However, this method produces very poor results at low temperatures. We have thus used a ME method to compute C_v as proposed in Ref. 40. In Fig. 24, we show $C_v(T)$ as well as the uniform spin an charge susceptibilities for various couplings as a function of temperature.

At $J/t=0$, the specific heat is given by the sum of a delta function at $T=0$ for the localized spins and the specific heat of free fermions. By switching on the coupling, they are combined to form a two-peak structure. The broad peak at high-temperature $T\sim t$ is almost independent of the coupling J and is rather similar to the free-electron gas. The sharp peak at lower temperatures strongly depends on the exchange constant. It shifts toward higher temperatures and becomes broader with increasing J/t. The location of this peak tracks the magnetic scale T_S indicating that its origin comes from the spin excitations. In the spin gapped phase, we note that the overall features of C_v agree with the 1D case.[41]

V. SUMMARY AND CONCLUSION

We have presented a detailed numerical study of ground-state and thermodynamic properties of the ferromagnetic and antiferromagnetic half filled KLM model on a square lattice. From the technical point of view, we have described and used an efficient (i.e., free of the minus-sign problem) auxiliary field QMC method to investigate the model. Both finite and ground-state algorithms were discussed. The approach is by no means restricted to the KLM and may be applied to investigate models such as the half filled two channel Kondo lattice or various forms of depleted Kondo lattices in which the impurity spins are removed in a regular or random way. However, we are tied to particle-hole symmetry, since only in this case can we avoid the minus-sign problem.

In two dimensions, the KLM shows a quantum phase transition between antiferromagnetically ordered and disordered states. This transition occurs at $J/t=1.45\pm0.05$. The magnon dispersion evolves smoothly from its strong coupling form with spin gap at $\vec{Q}=(\pi,\pi)$ to a spin-wave form in the ordered phase. The transition may be well understood in the framework of a bond-operator mean-field approximation of the Kondo necklace model.[33] Here, the disordered phase is represented by a condensation of singlets with an energy gap at $\vec{Q}=(\pi,\pi)$ for magnon excitations. At and below the critical point, the spin gap closes, leading to a condensation of both singlets and triplets at the antiferromagnetic wave vector. The system remains insulating. To a first approximation and as in the one-dimensional case, the quasiparticle gap scales a $|J|$ irrespective of the sign of J. In

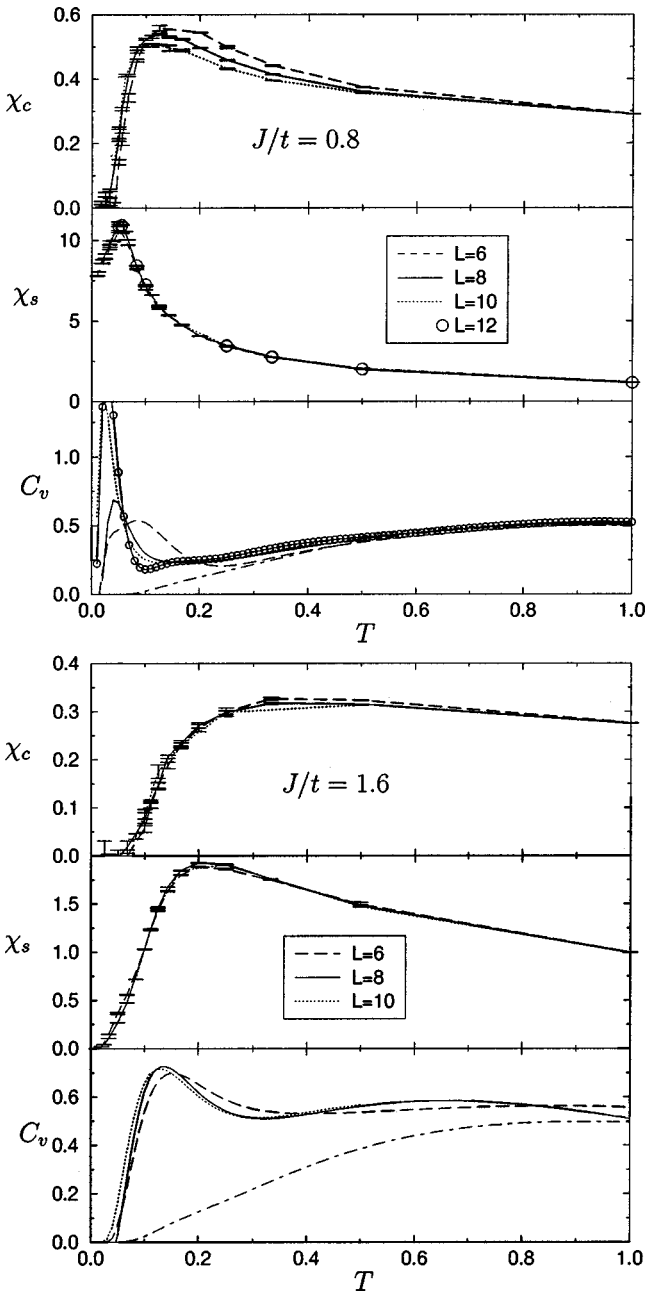

FIG. 24. Spin χ_s and charge χ_c susceptibilities as well as specific heat C_v as a function of temperature for various values of J/t. The dot-dashed line represents the specific heat of free electrons on $L=8$.

contrast, the quasiparticle dispersion relation shows marked differences between ferromagnetic and antiferromagnetic couplings. For antiferromagnetic couplings the quasiparticle dispersion always has a structure that follows the functional form obtained in the noninteracting PAM: $E_{\pm}(\vec{k})=\frac{1}{2}(\varepsilon(\vec{k}) \pm \sqrt{\varepsilon(\vec{k})^2+\Delta^2})$. This functional form is obtained in various approximations[34,42] that take into account Kondo screening but neglect magnetic ordering. In the antiferromagnetic phase, the above dispersion relation is merely supplemented by shadow features. One obtains a four-band structure that is well reproduced by mean-field theories that produce phases with coexistence of magnetic ordering and Kondo screening.[34] Thus, in the ordered phase, screening of the impurities is not complete. The remnant magnetic moments order due to the RKKY interaction. Although we cannot dope the system—due to severe minus-sign problems—it is tempting to assume a rigid band picture and to describe the doped phase by shifting the chemical potential into the conduction band. Since the quasiparticle gap is determined by the $\vec{k}=(\pm\pi,\pm\pi)$ points, the Fermi line will consist of hole pockets around those points and one expects the Luttinger volume to account both for localized and conduction electrons. Furthermore, since the band is very flat around those points, a larger effective mass is anticipated. Ferromagnetic couplings show a different behavior. In this case, Kondo screening is absent but the RKKY interaction present. The quasiparticle dispersion is well fitted by the form $E_{\pm}(\vec{k})=\pm\sqrt{\varepsilon(\vec{k})^2+\Delta^2}$ corresponding to free electrons subject to an external staggered magnetic field. In this case, again assuming a rigid band picture, doping produces a Luttinger volume containing only the conduction electrons. This contrasting behavior of the Luttinger volume for the ferromagnetic and antiferromagnetic KLM is reproduced in the limit of large dimensions.[11]

From the finite-temperature simulations, we can define spin T_S and charge T_C energy scales by locating the maximum in the charge and spin susceptibilities. From weak to intermediate couplings, the spin scale follows a J^2 law, in agreement with the energy scale associated with the RKKY interaction. At strong couplings, $T_S \propto J$,. In contrast, both in the weak- and strong-coupling limit, $T_C \sim J$. In the range where $T_S \propto J^2$, the staggered susceptibility shows a marked increase at $T \sim T_S$. Hence, in this range T_S corresponds to the onset of antiferromagnetic fluctuations. On the other hand, the charge scale determines to a first approximation the minimum in the resistivity. Furthermore, at T_C antiferromagnetic intracell correlations between the *f* and *c* electrons are formed and a dip in the integrated density of states $N(\omega)$ at the Fermi level is observed. Thus, this scale marks the onset of enhanced scattering originating from the screening of the magnetic impurities. In the limit of infinite dimensions, a similar behavior in the charge degrees of freedom is seen, but at a much smaller energy scale, $T_0 \sim e^{-1/2JN(\varepsilon_f)}$.[10] Apart from a factor 1/2 in the exponent, T_0 corresponds to Kondo temperature of the single impurity problem. In one dimension, a dip in $N(\omega)$ is observed at an energy scale larger than the spin gap that scales as $e^{-1/\alpha JN(\varepsilon_f)}$ in the weak-coupling limit [with a numerical estimation of $1 \leqslant \alpha \leqslant 5/4$ (Ref. 15) or $\alpha=1.4$ (Ref. 16)].

In the weak-coupling limit, one can analyze the single-particle spectral function at various temperatures. Our results show that the quasiparticle gap of order *J* is formed only at the magnetic energy scale. Thus, one can only conclude that the quasiparticle gap at weak couplings is of magnetic origin. In contrast, at strong coupling, the quasiparticle gap originates from Kondo screening. The above stands in agreement with arguments and numerical results presented for the one-dimensional (1D) case.[15,16] At weak couplings in one dimension the spin gap becomes exponentially small. Hence, the time scale associated with magnetic fluctuations is exponentially larger than the time scale relevant for charge fluctuations that is set by *t*. The conduction electrons thus effectively feel a static magnetic ordering. In one dimension and in 2D, in the presence of particle-hole symmetry, nesting of the noninteracting Fermi surface is present. At a mean-field level and in the presence of magnetic ordering, this leads to a quasiparticle gap $\Delta_{qp}=J/4$. In 2D, one may alter the shape of the noninteracting Fermi surface so as to avoid nesting by introducing a small nearest-neighbor hopping matrix element. In this case, the mean-field approximation does not produce an insulating state in the presence of antiferromagnetic ordering. Since nesting is related to particle-hole symmetry, we cannot address this question in the QMC approach due to severe sign problems. Hence, it is worth paying particular attention to our results at weak couplings and $T_C > T > T_S$, before antiferromagnetic correlations set in. Here, Kondo screening is present but antiferromagnetic correlations absent. In this temperature range, $A(\vec{k},\omega)$ shows a dispersion relation following that of hybridized bands with the quasiparticle gap lying beyond our resolution.

We have equally computed the specific heat, C_v. This quantity shows a two-*peak* structure. The broad high-energy ($T \sim t$) feature stems from the conduction electrons. The low-energy peak is very sharp in the ordered phase and tracks T_S. It is hence of magnetic origin.

Finally, we discuss the relationship of our results to experiments. Let us first concentrate on $Ce_3Bi_4Pt_3$. At $T=100$ K the effective magnetic moment of Ce ions starts decreasing.[43] At higher temperatures, the Ce ion has a next to fully developed moment (i.e., $J=5/2$ as appropriate for Ce^{3+}). At the same temperature scale, the real part of the optical conductivity shows a reduction of spectral weight in a frequency range of 39 meV or 450 K.[43,44] Those results imply that the opening of a gap is related to the screening of magnetic impurities and hence, the KLM seems to be an adequate prototype model for the description of this class of materials. The above-described temperature evolution is precisely seen in our numerical simulations. At $T \simeq T_C$ and at *weak* couplings, the optical conductivity shows a transfer of spectral weight from low frequencies to frequencies well above T_C (Fig. 11). Screening of the magnetic moments start equally at $T \simeq T_C$ (Fig. 13). For the above material, the optical gap is estimated by $\Delta_\sigma=39$ meV (Ref. 45) and photoemission experiments suggest a quasiparticle gap $\Delta_{qp}=20$ meV.[46] At a temperature scale $T \simeq 25$ K, a gap in the mag-

netic excitation of $\Delta_{sp}=12$ meV is observed. Those small energy scales imply that small values of J/t should be considered. The gaps equally satisfy the relation $\Delta_c \simeq 2\Delta_{qp} > \Delta_{sp}$ as obtained in the KLM. Hence, one should place this material in the parameter range $J>J_c$, which in our calculations seem rather large in comparison to the small charge gap observed in experiments. However, one should keep in mind that J_c may be sensitive to the properties of the noninteracting Fermi surface. In particular nesting—which is present in our calculation—will certainly enhance the value of J_c. We now turn our attention to CeNiSn. CeNiSn has a transport gap roughly an order of magnitude smaller than $Ce_3Bi_4Pt_3$, and hence—assuming a KLM description of the material—should correspond to smaller values of J/t in comparison to $Ce_3Bi_4Pt_3$. (Note that recent measurements down to ~ 0.1 K have found an electronic contribution to the specific heat.[47] This is interpreted in terms of a finite density of states within the gap.) This smaller value of J/t leads to signs of magnetism. Indeed, along the *a* axis of the orthorhombic structure, CeNiSn shows a peak in the magnetic susceptibility at 12 K. At the same energy scale, an anomaly is seen in the specific heat.[48] This seems consistent with our results.

ACKNOWLEDGMENTS

We acknowledge useful discussions and communications with R. Eder, M. Feldbacher, G. Grüner, O. Gunnarson, C. Huscroft, Y. Lu, A. Muramatsu, H. Tsunetsugu, and G. M. Zhang. We thank HLRS Stuttgart for generous allocation of CPU time on the Cray-T3E.

[1] P. A. Lee, T. M. Rice, J. W. Serene, L. J. Sham, and J. W. Wilkins, Comments Condens. Matter Phys. **12**, 99 (1986).
[2] G. Aeppli and Z. Fisk, Comments Condens. Matter Phys. **16**, 155 (1992).
[3] J. R. Schrieffer and P. A. Wolff, Phys. Rev. **149**, 491 (1966).
[4] M. Imada, A. Fujimori, and Y. Tokura, Rev. Mod. Phys. **70**, 1039 (1998).
[5] A. C. Hewson, *The Kondo Problem to Heavy Fermions, Cambridge Studies in Magnetism* (Cambridge University Press, Cambridge, 1997).
[6] J. Kondo, Prog. Theor. Phys. **32**, 37 (1964).
[7] P. W. Anderson, Phys. Rev. **164**, 352 (1967).
[8] C. Kittel, *Quantum Theory of Solids* (Wiley, New York, 1963).
[9] S. Doniach, Physica B **91**, 231 (1977).
[10] M. Jarrell, Phys. Rev. B **51**, 7429 (1995).
[11] N. Matsumoto and F. J. Ohkawa, Phys. Rev. B **51**, 4110 (1995).
[12] T. M. Rice and K. Ueda, Phys. Rev. B **34**, 6420 (1986).
[13] M. Vekic, J. W. Cannon, D. J. Scalapino, R. T. Scalettar, and R. L. Sugar, Phys. Rev. Lett. **74**, 2367 (1995).
[14] C. Gröber and R. Eder, cond-mat/9909008 (unpublished).
[15] H. Tsunetsugu, M. Sigrist, and K. Ueda, Rev. Mod. Phys. **69**, 809 (1997).
[16] N. Shibata and K. Ueda, J. Phys.: Condens. Matter **11**, R1 (1999).
[17] R. Blankenbecler, D. J. Scalapino, and R. L. Sugar, Phys. Rev. D **24**, 2278 (1981).
[18] M. Jarrell and J. Gubernatis, Phys. Rep. **269**, 133 (1996).
[19] R. M. Fye and D. J. Scalapino, Phys. Rev. Lett. **65**, 3177 (1990).
[20] R. M. Fye and D. J. Scalapino, Phys. Rev. B **44**, 7486 (1991).
[21] R. M. Fye, Phys. Rev. B **33**, 6271 (1986).
[22] F. F. Assaad, W. Hanke, and D. J. Scalapino, Phys. Rev. B **50**, 12 835 (1994).
[23] F. F. Assaad, M. Imada, and D. J. Scalapino, Phys. Rev. B **56**, 15 001 (1997).
[24] F. F. Assaad and M. Imada, J. Phys. Soc. Jpn. **65**, 189 (1996).
[25] M. Feldbacher and F. F. Assaad, Phys. Rev. B **63**, 73105 (2001).
[26] E. Loh and J. Gubernatis, in *Modern Problems of Condensed Matter Physics*, edited by W. Hanke and Y. V. Kopaev (North-Holland, Amsterdam, 1992), Vol. 32, p. 177.
[27] S. Q. Shen, Phys. Rev. B **53**, 14 252 (1996).
[28] H. Tsunetsugu, Phys. Rev. B **55**, 3042 (1997).
[29] J. E. Hirsch, Phys. Rev. B **28**, 4059 (1983).
[30] F. F. Assaad, in *High Performance Computing in Science and Engineering*, edited by E. Krause and W. Jäger (Springer, Berlin, 1998), p. 105; cond-mat/9806307 (unpublished).
[31] F. F. Assaad, Phys. Rev. Lett. **83**, 796 (1999).
[32] S. Sachdev and R. N. Bhatt, Phys. Rev. B **41**, 9323 (1990).
[33] G.-M. Zhang, Q. Giu, and L. Yu, Phys. Rev. B **62**, 69 (2000).
[34] G.-M. Zhang and L. Yu, Phys. Rev. B **62**, 76 (2000).
[35] O. Gunnarsson and J. E. Han, Nature (London) **405**, 1027 (2000).
[36] S. Chakravarty, B. I. Halperin, and D. R. Nelson, Phys. Rev. Lett. **60**, 1057 (1988).
[37] S. Chakravarty, B. I. Halperin, and D. R. Nelson, Phys. Rev. B **39**, 2344 (1989).
[38] K. Haule, J. Bonča, and P. Prelovšek, Phys. Rev. B **61**, 2482 (2000).
[39] N. Read and D. N. Newns, J. Phys. C **16**, 3273 (1983).
[40] C. Huscroft, R. Gass, and M. Jarrell, Phys. Rev. B **61**, 9300 (2000).
[41] N. Shibata, B. Ammon, M. Troyer, M. Sigrist, and K. Ueda, J. Phys. Soc. Jpn. **67**, 1086 (1998).
[42] R. Eder, O. Rogojanu, and G. A. Sawatzky, Phys. Rev. B **58**, 7599 (1998).
[43] B. Bucher, Z. Schlesinger, P. C. Canfield, and Z. Fisk, Phys. Rev. Lett. **72**, 522 (1994).
[44] L. Degiorgi, Rev. Mod. Phys. **71**, 687 (1999).
[45] A. Severing, J. D. Thompson, P. C. Canfield, Z. Fisk, and P. Riseborough, Phys. Rev. B **44**, 6832 (1991).
[46] K. Breuer, S. Messerli, D. Purdie, M. Garnier, M. Hengesberger, G. Panaccione, Y. Baer, T. Takahashi, S. Yoshi, M. Kasaya, K. Katoh, and T. Takabatake, Europhys. Lett. **41**, 565 (1998).
[47] K. Izawa, T. Suzuki, T. Fujita, T. Takabatake, G. Nakamoto, H. Fujii, and K. Maezawa, Phys. Rev. B **59**, 2599 (1999).
[48] T. Takabatake, F. Teshima, H. Fujii, S. Nishigori, T. Suzuki, T. Fujita, Y. Yamaguchi, J. Sakurai, and D. Jaccard, Phys. Rev. B **41**, 9607 (1990).